UNIVERSITY OF SOUTHERN CALIFORNIA
Department of Civil Engineering

IMPULSE RESPONSE ANALYSIS OF THE VAN NUYS 7-STORY HOTEL DURING 11 EARTHQUAKES (1971-1994): ONE-DIMENSIONAL WAVE PROPAGATION AND INFERENCES ON GLOBAL AND LOCAL REDUCTION OF STIFFNESS DUE TO EARTHQUAKE DAMAGE

by

Maria I. Todorovska and Mihailo D. Trifunac

Report CE 06-01

July, 2006
Los Angeles, California

www.usc.edu/dept/civil_eng/Earthquake_eng/

ABSTRACT

The Van Nuys 7-story hotel, located in the Los Angeles metropolitan area, is a rare example of an instrumented reinforced concrete building that has been damaged by earthquakes. It was damaged by two earthquakes – 1971 San Fernando, and 1994 Northridge, both of which were recorded in the building. In addition, strong motion data of other 10 earthquakes, which occurred over a 24 year period (1971-1994), are available. These recordings are invaluable for validation of structural health monitoring methods. In this report we present an analysis for one such method, and using the EW response of this building during 11 earthquakes.

Wave travel times of vertically propagating waves are measured from plots of impulse response functions computed by deconvolution of the recorded earthquake response. The changes in wave travel times are used to infer the local (between sensors) and global changes of structural stiffness, from one event to another, and with time during the earthquakes that damaged the building (San Fernando and Northridge). The measured wave travel times are also used to estimate the fundamental fixed-base frequency of the building, f_1. These estimates of f_1 are compared with independent estimates of the soil-structure system frequency f_{sys} during the same earthquakes and during five ambient vibration tests, and are all found to be mutually consistent. For this building, f_1 during strong longitudinal (EW) motion changed between 1.35 Hz (at the beginning of the San Fernando earthquake) and 0.66 Hz (during the intervals of strongest shaking by the Northridge earthquake).

For three of the earthquakes, which produced the largest response (1971 San Fernando, 1994 Northridge, and 1992 Landers), the analysis is conducted for several time intervals, and changes in stiffness are detected relative to the initial time interval. The analysis shows that monitoring only the changes of f_{sys} can be misleading for structural health monitoring and can lead to erroneous alarms, while monitoring changes of f_1 over suitably chosen time windows (before, during, and after excitation by strong earthquake motions) can be a powerful and robust tool for structural health monitoring. It is concluded that, under favorable conditions, this method can be used as a tool for structural health monitoring, provided the threshold changes in the system properties have been properly calibrated in terms of actually observed damage.

Keywords: Earthquake response, Damage Detection, Structural health monitoring, wave propagation times, Impulse response function, Van Nuys hotel.

TABLE OF CONTENTS

1. INTRODUCTION

Validation of structural health monitoring methods is best done in terms of data of full-scale response of structures to actual earthquake excitation. Data from *multiple* earthquake excitations in a structure are particularly valuable. Such data are however limited, rarely sufficient, and almost never complete to allow unequivocal and unique interpretation. The Van Nuys 7-story hotel building is a rare example of an instrumented reinforced concrete building damaged by earthquakes. What is particularly valuable about this building is that strong motion data from about dozen earthquakes are available over a period of 24 years (between February of 1971 and December of 1994), two of which caused visible damage. Five ambient vibration tests of the building have also been conducted, two of which have been comprehensive and well documented. This work presents an application of a structural health monitoring method based on detecting changes in wave travel times through this building. The evolution of damage is described using wave travel times measured from plots of impulse response functions computed from the recorded seismic response in different time windows – before, during and after the intervals of the strong shaking.

For structures supported by soils, typical for most metropolitan areas, the soil-structure interaction is an integral part of the dynamic response. For a soil-structure system, the peaks of the building relative response transfer-function occur at the frequencies of the soil-structure system, rather than at the building fixed-base frequencies. Although the two sets of frequencies are related, it is difficult to determine the fixed-base frequencies, which are those that are directly related to loss of structural stiffness, from recorded seismic response, unless the structure is appropriately instrumented. At present, the configuration of instruments in typical buildings is incomplete for soil-structure interaction studies. Consequently, changes of f_{sys} – the first frequency of the soil-structure system, have often been erroneously interpreted to be *entirely* due to loss of structural stiffness. For comprehensive and reliable health monitoring it is essential to be able to monitor f_1 – the fundamental fixed-base frequency – separately from f_{sys} – the first frequency of the soil-structure system.

Recently, Snieder and Şafak (2006) used impulse response functions, computed by deconvolution from small amplitude seismic response, to analyze one-dimensional wave propagation in Millikan Library in Pasadena, California. They estimated f_1 from the travel time of shear waves to propagate along the building height, which required recorded horizontal motion only at the ground floor and at the roof. In this work, we apply the same procedure – to estimate f_1 from incomplete data – to the EW response of the Van Nuys building during 11 of the earthquakes recorded in the building. We estimate the variations of f_1 from one earthquake to another, and during the earthquakes that caused damage, and *calibrate* the detected changes in

terms of the observed and documented damage. Such calibration is essential for using f_1 as a robust tool for real time structural health monitoring. We applied the same procedure earlier to estimate f_1 for the Imperial County Services Building – a 6-story reinforced concrete structure in El Centro, California – severely damaged by the Imperial Valley earthquake of October 15, 1979, and later demolished – and analyzed the changes in f_1 as function of the level of response, and in relation to f_{sys} and the observed damage (Todorovska and Trifunac 2006c). For that building, only records of the Imperial Valley earthquake were available.

Changes in f_1 reflect changes in the *global* stiffness of the structure. Due to the redundancy of civil engineering structures, however, changes in the global stiffness may be small if the damage is localized, and, hence, difficult to detect in "noisy" data, where "noise" refers to changes due to factors other than damage (see Chang et al., 2003, and Doebling et al., 1996, for detailed state of the art reviews on this topic). Wave propagation methods, however, make it possible to detect local changes in stiffness, with relatively few sensors, by detecting changes in travel times of seismic waves between sensors. In this work we also estimate *local* changes in stiffness of the Van Nuys building during the San Fernando and Northridge earthquakes, using impulse responses to measure changes in wave travel times.

There have been only a few publications in literature on wave propagation methods, other than nondestructive testing, for structural health monitoring and damage detection in civil structures. Şafak (1999) proposed a layered continuous model for analysis of seismic response of a building, and detection of damage by tracing changes in the parameters in the layers. Ivanović et al. (2001) and Trifunac et al. (2003) used strong motion data recorded in a 7-story RC building in Van Nuys during the 1994 Northridge earthquake, to explore two methods, one based on cross-correlation analysis (to estimate time lags between motions recorded at different levels), and the other one based on detecting changes in wave numbers (inversely proportional to the wave velocities) of waves propagating between different levels. Ma and Pines (2003) proposed a method based on a lumped mass building model, and propagation of dereverberated waves to identify the damage, which they tested on simulated building response data. The first application of the impulse response functions computed by deconvolution (Snieder and Şafak 2006)), to detect local changes in stiffness, and for earthquake damage detection in general, appears to be our recent study of the Imperial County Services building (Todorovska and Trifunac 2006c).

In this report, we first present a brief description of the building, available strong motion data, and the reported damage (included for completeness of this presentation). This is followed by a review of the methodology and presentation of the results, analysis, and conclusions.

2. THE BUILDING

The structure we study is a seven-story hotel building located in Van Nuys, California, referred to in this work as VN7SH. Its damage following San Fernando, 1971, and Northridge, 1994, earthquakes has been described in numerous papers and reports (Blume et al. 1973; Ivanović et al. 1999; Trifunac and Hao 2001; Trifunac et al. 1999a,b).

Location. The VN7SH is located in central San Fernando Valley of the Los Angeles metropolitan area (at 34.221^{o} N and 118.471^{o} W), north-west from downtown Los Angeles. Figure 2.1 shows San Fernando Valley and the building location, relative to the major freeways and to the horizontal projections of the fault planes of 1971 San Fernando and 1994 Northridge earthquakes (Trifunac 1974; Wald and Heaton 1996), which both damaged the building and were recorded in the building, the epicenters of two Northridge aftershocks, and directions and epicentral distances to seven other earthquakes recorded in the building (Trifunac et al. 1999b).

Design. The building was designed in 1965, and constructed in 1966 (Blume et al. 1973; Mulhern and Maley 1973). Figure 2.2 shows: (a) a plan view of a typical floor, (b) the foundation layout, (c) a side view of the building frame, and (d) a typical soil-boring log data at the building site. The building is 19.1 × 45.7 m in plan. The typical framing consists of columns spaced at 6.35 m centers in the transverse direction, and 5.72 m centers in the longitudinal direction. Spandrel beams surround the perimeter of the structure. The properties of the construction materials are listed in Table 2.1.

Lateral forces in each direction are resisted by interior column-slab frames and exterior column spandrel beam frames. The added stiffness in the exterior frames associated with the spandrel beams creates exterior frames that are roughly twice as stiff as the interior frames. The floor system is reinforced concrete flat slab, 25.4 cm thick at the second floor, 21.6 cm thick at the third to seventh floors and 20.3 cm thick at the roof (Browning et al. 2000; De La Llera et al. 2000; Islam 1996; Trifunac and Ivanović 2003; Li and Jirsa 1998).

Site Conditions. The building is situated on undifferentiated Holocene alluvium, uncemented and unconsolidated, with thickness < 30 m, and age < 10,000 years (Trifunac and Todorovska 1998). The average shear wave velocity in the top 30 m of soil is 300 m/s. The soil-boring log in Fig. 2.2d shows that the underlying soil consists primarily of fine sandy silts and silty fine sands. The foundation system (Fig. 2.2b) consists of 96.5 cm deep pile caps, supported by groups of two to four poured-in-place 61 cm diameter reinforced concrete friction piles. These are centered under the main building columns. The pile caps are connected by a grid of beams. Each pile is roughly 12.2 m long, and has design capacity of over 444.82 × 10^3 N for vertical load, and up to 88.96 × 10^3 N for lateral load. The structure is constructed of normal weight reinforced concrete (Blume and Assoc. 1973).

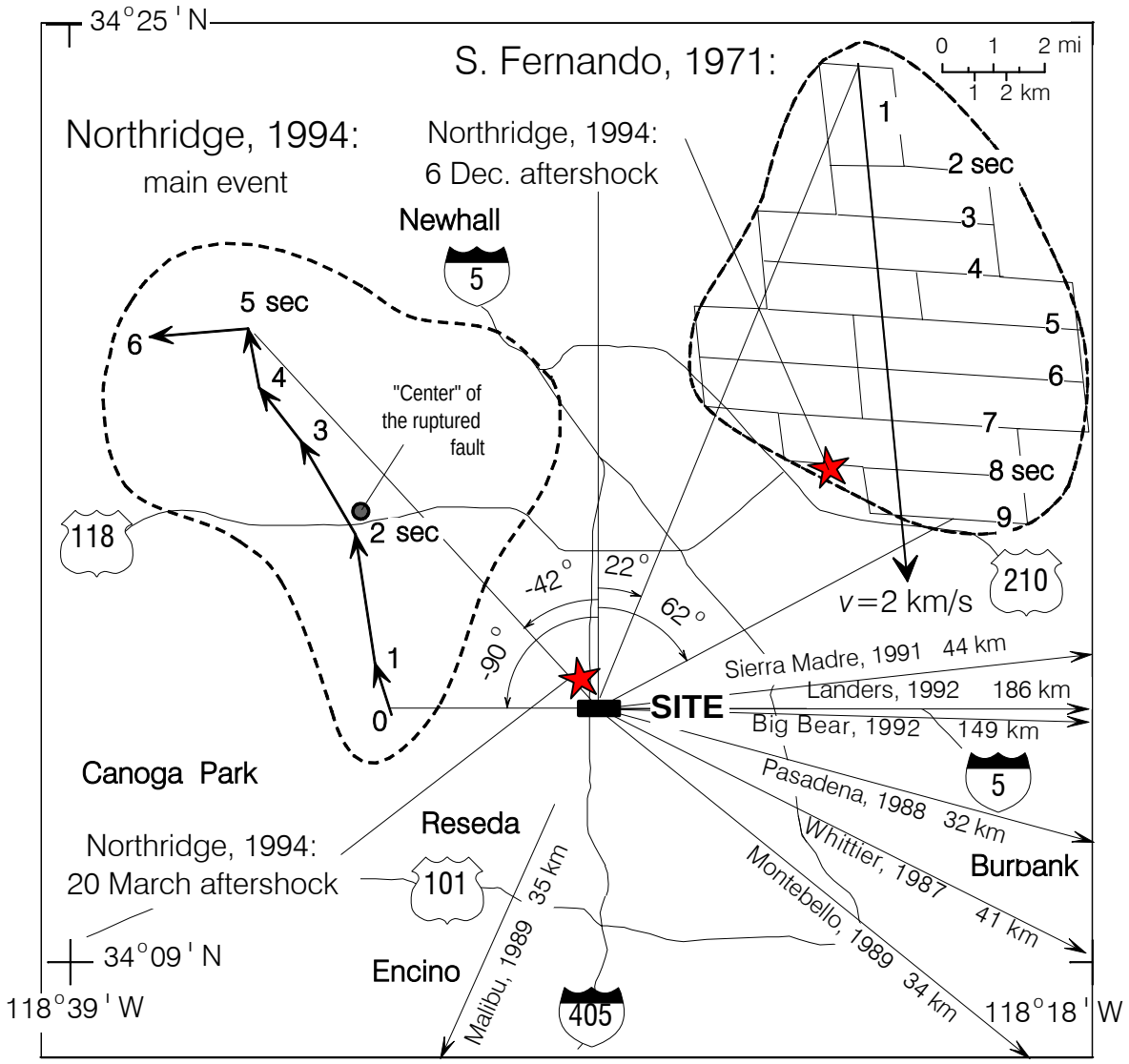

Fig. 2.1 General setting of the Van Nuys building site in central San Fernando Valley. The location of the building relative to the fault planes of the 1971 San Fernando and 1994 Northridge earthquakes (their horizontal projections are shown by dashed lines), the epicenters of two Northridge aftershocks (solid stars) and other earthquakes with epicenters outside the map are also shown.

Earthquake Damage. The M_L = 6.6 San Fernando earthquake of February 9, 1971, caused minor structural damage (Blume and Assoc., 1973). Epoxy was used to repair the spalled concrete of the second floor beam-column joints on the North side and East end of the building. The recorded peak accelerations in the building along the longitudinal (L), transverse (T) and vertical (V) axes of symmetry were: 0.13g (L), 0.24g (T) and 0.18g (V) at the base, and 0.32g (L), 0.39g (T) and 0.22g (V) at the roof.

Table 2.1 Properties of the construction materials of the VN7SH building

Concrete (regular weight, 150 pcf [1])		
Location in the structure	Minimum specified compressive strength f_c' – psi [2]	Modulus of elasticity E – psi [2]
Columns, 1st to 2nd floors	5,000	4.2×10^6
Columns, 2nd to 3rd floors	4,000	3.7×10^6
Beams and slabs, 2nd floor	4,000	3.7×10^6
All other concrete, 3rd floor to roof	3,000	3.3×10^6

Reinforcing steel			
Location in the structure	Grade	Minimum specified yield strength f_y – ksi [3]	Modulus of elasticity E – psi [2]
Beams and slabs	Intermediate grade deformed billet bars (ASTM A-15 and A-305)	40	29×10^6
Column bars	Deformed billet bars (ASTM A-432)	60	29×10^6

[1] Pounds per cubic foot
[2] Pounds per square inch
[3] Kips per square inch

The M_L = 6.4 Northridge earthquake of January17, 1994, severely damaged the building. The structural damage was extensive in the exterior north (D) and south (A) frames, designed to take most of the lateral load in the longitudinal (EW) direction. Severe shear cracks occurred at the middle columns of frame A, near the contact with the spandrel beam of the 5th floor (Fig. 2.3 and 2.4). Those cracks significantly decreased the axial, moment, and shear capacity of the columns. The shear cracks which appeared in the north (D) frame on the 3rd and 4th floors, and the damage of columns D2, D3 and D4 on the 1st floor caused minor to moderate changes in the capacity of these structural elements. No major damage of the interior longitudinal (B and C) frames was observed. There was no visible damage in the slabs and around the foundation. The nonstructural damage was significant. The recorded peak accelerations in the building along the longitudinal (L), transverse (T) and vertical (V) axes of symmetry were: 0.46g (L), 0.40g (T) and 0.28g (V) at the base, and 0.59g (L) and 0.58g (T) at the roof (there were no sensors installed on the roof to measure vertical motions). The motions in the area surrounding the building (determined from smoothed contour maps) had relatively small horizontal transient peak accelerations, *a*,

velocities, v, and displacements, d (a_R=–350 cm/s^2 , a_T=225 cm/s^2, a_V=600 cm/s^2, v_R=–40 cm/s, v_T=30 cm/s, v_V=–25 cm/s, d_R=–14 cm, d_T=25 cm, d_V=–7 cm; subscripts R, T and V refer to radial, transverse and vertical components, defined relative to point 34.27º N and 118.55º W in the "center" of the ruptured area, see Fig. 2.1, and positive if away from the fault, clockwise and upward) (Trifunac et al. 1994, Todorovska and Trifunac 1997a,b). In the vicinity of the building, the peak strain factor was: horizontal ~$10^{-2.6}$ and vertical ~$10^{-3.2}$ (Trifunac et al., 1996, Trifunac and Todorovska, 1999). The (refined) estimate of Modified Mercalli intensity at the site was VIII (Trifunac and Todorovska, 1997a,b; 2001).

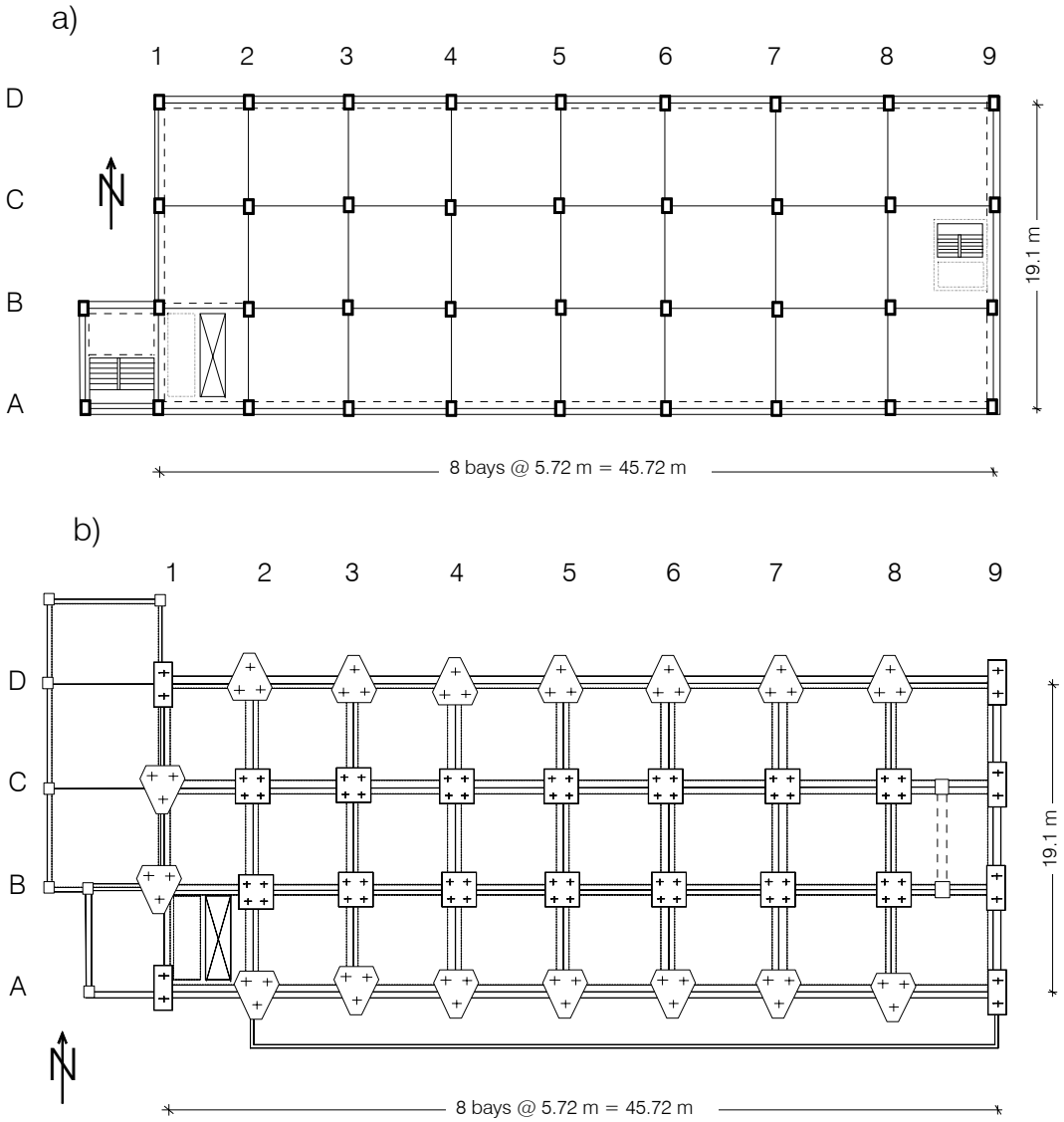

Fig. 2.2 VN7SH building: (a) typical floor plan, (b) foundation plan, (c) typical transverse section, and (d) soil boring data from 7/17/1965.

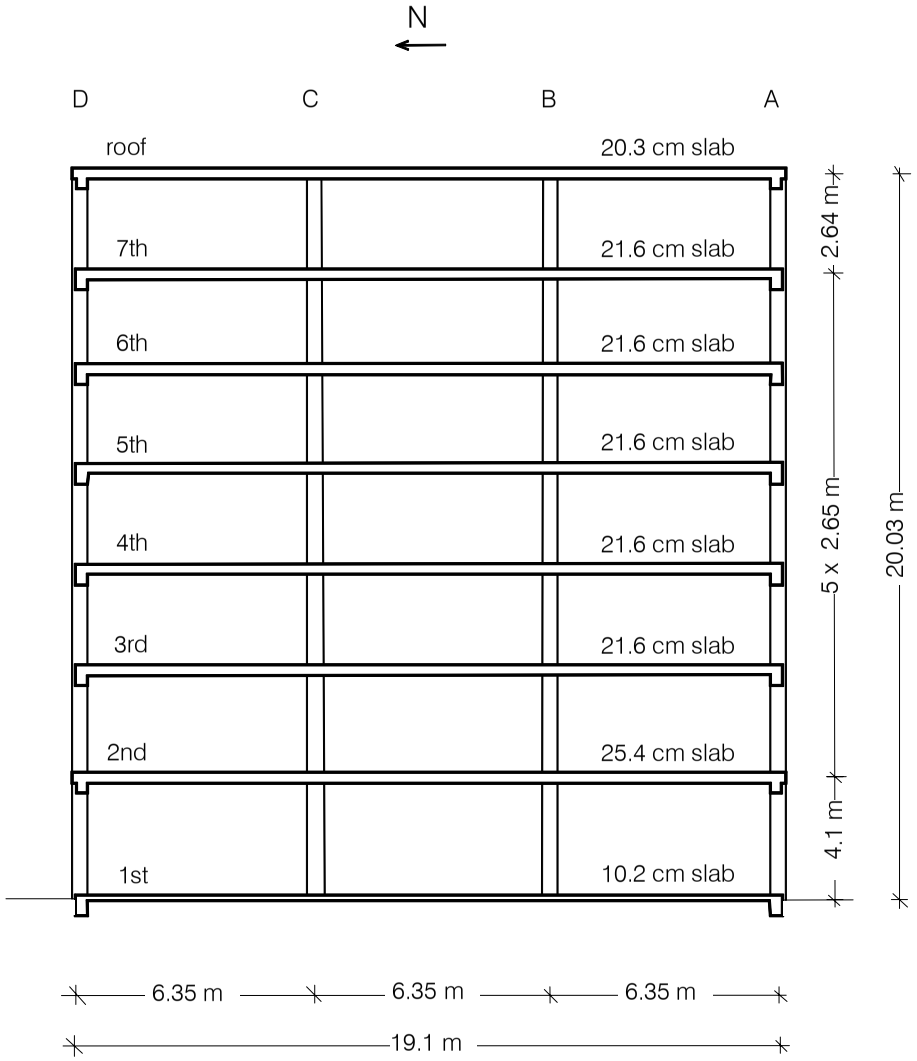

c)

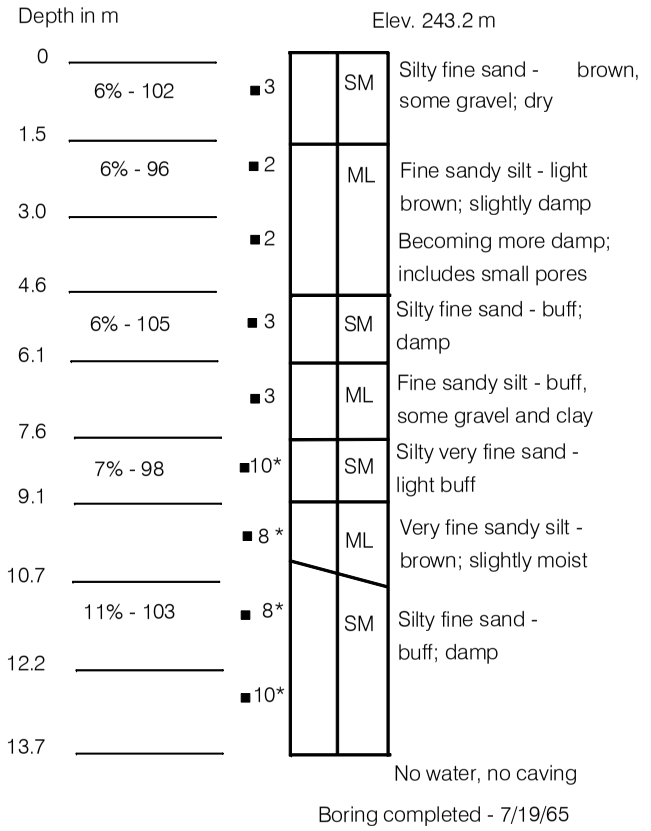

LEGEND :

A Field moisture expressed as a percentage of the dry weight soil.

B Dry density expressed in pounds per cubic foot.

C Blows per foot of penetration using a 17.8×10^{3} N hammer dropping 30.5 cm

* - a 17.8×10^{3} N hammer was used.

■ Depth at which undesturbed sample was extracted.

d)

Fig. 2.2 (cont.).

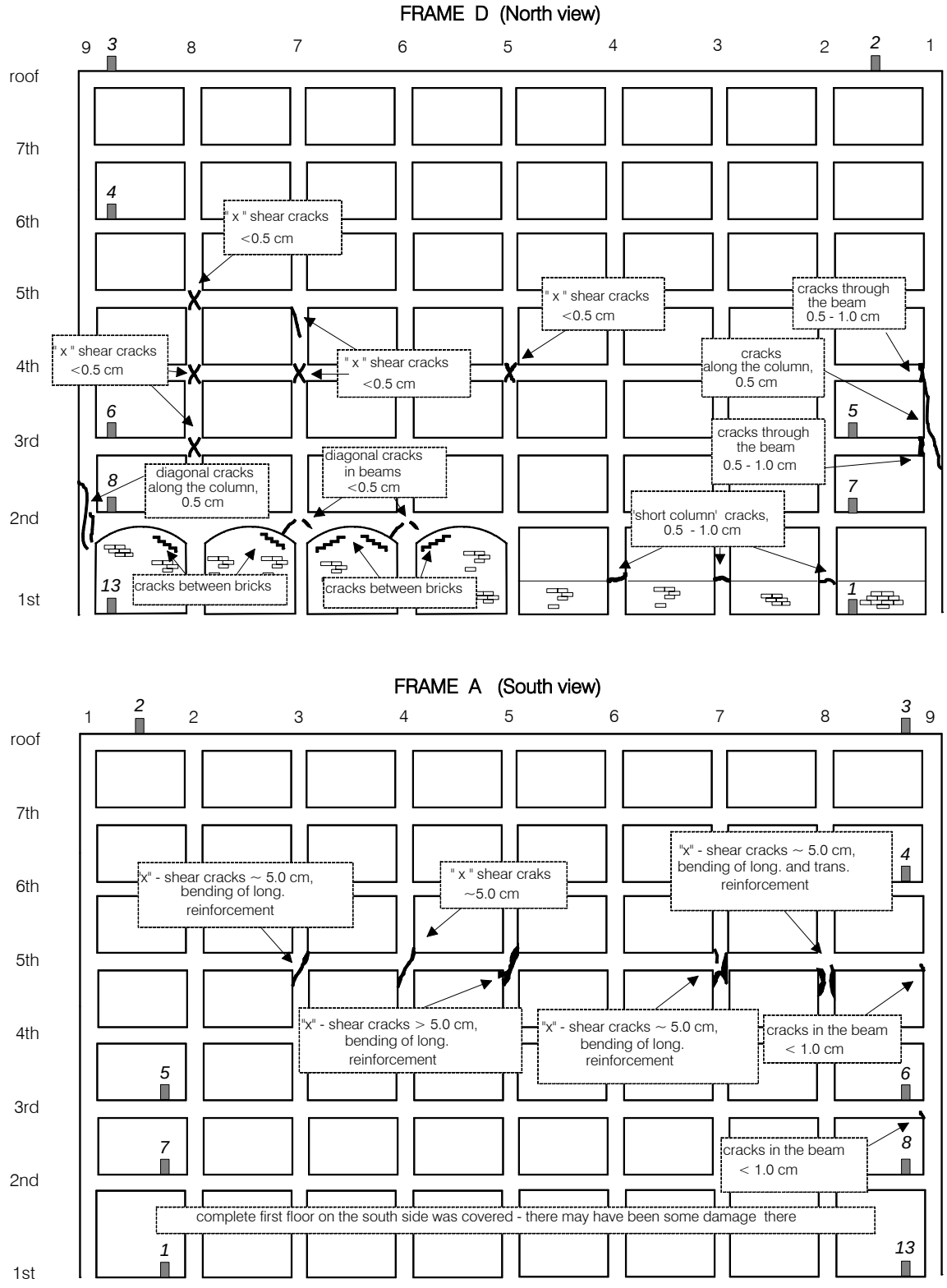

Fig. 2.3 Schematic representation of the damage: (top) frame D–North view, and (bottom) frame A–south view. The sensor locations for channels 1–8 and 13 (oriented towards North), are also shown (see Fig. 2.6).

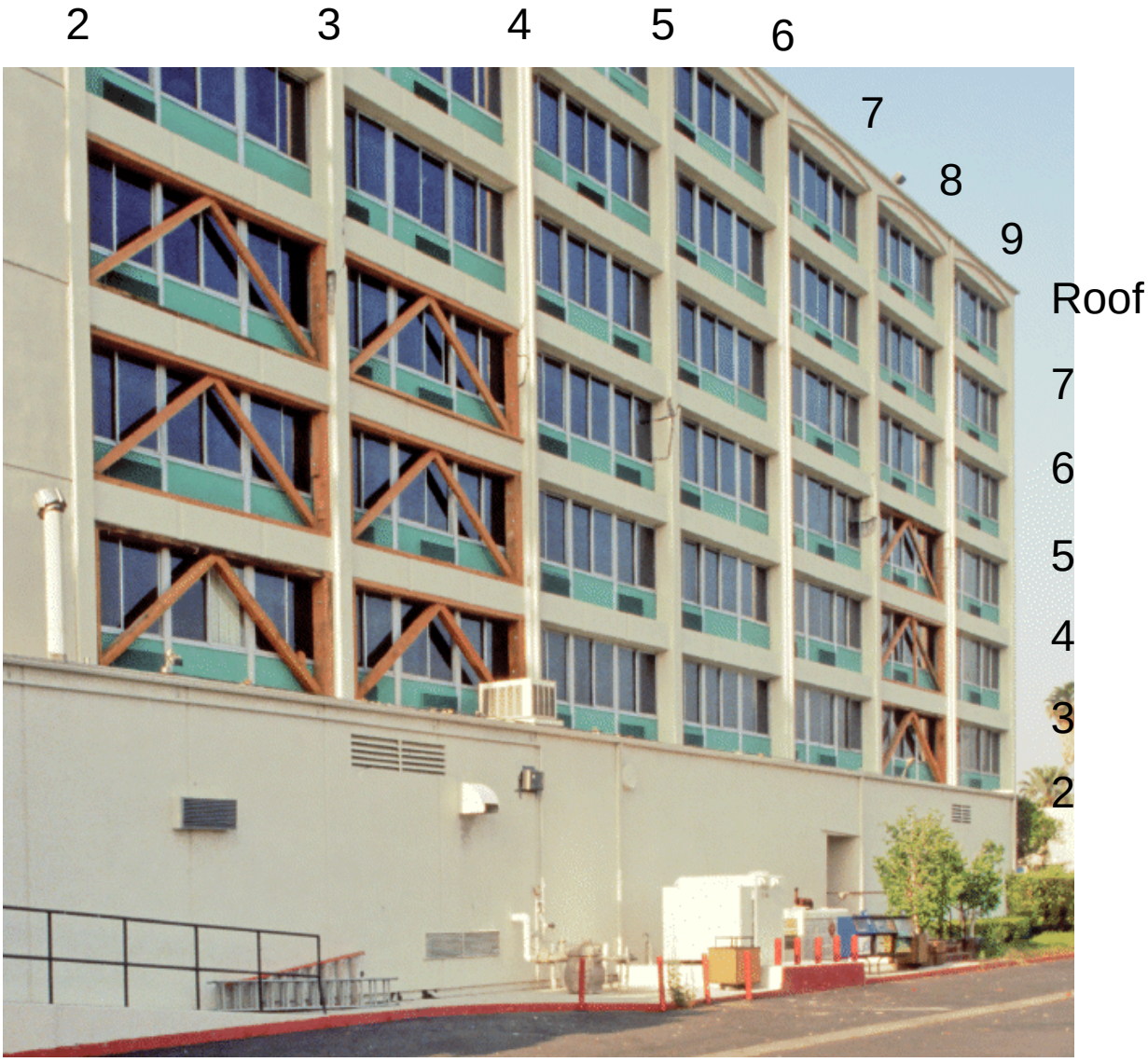

Fig. 2.4 South view of the Van Nuys building during the second ambient vibration test, of 5 Feb, 1994. Wooden braces in frame A are seen between columns 2 and 4, and 7 and 8.

Photographs and detailed description of the damage from the Northridge earthquake can be found in Trifunac et al. (1999b) and in Trifunac and Hao (2001). Analysis of the relationship between the observed damage and the changes in equivalent vertical shear wave velocity in the building, estimated from correlation of the recorded motions, can be found in Ivanović et al. (2001), and will be discussed again in the following pages. A discussion on the extent to which this damage has contributed to the changes in the apparent period of the soil-structure system can be found in Trifunac et al. (2001a,b)].

2.1 Ambient Vibration Experiments

The first ambient vibration survey of VN7SH was conducted in 1967, and again immediately after the San Fernando earthquake in 1971. The third test was conducted also in 1971 but after the building damage had been repaired. The measurements revealed that the first system period of EW response increased from 0.53 s before the earthquake to 0.72 s following the earthquake, and then deceased to 0.64 s following the repairs. The corresponding values of the first EW system frequency are 1.89 Hz, 1.39 Hz, and 1.56 Hz, and the change is a decrease by 26% and an increase by 12% following repair. For NS vibrations, the system period increased from 0.48 s before the earthquake to 0.68 s after the earthquake, and then it decreased to 0.58 s after the repairs. The corresponding values of the first NS system frequency are 2.08 Hz, 1.47 Hz, and 1.72 Hz, and the changes are a decrease by 29% and an increase by 17% (Mulhern and Maley 1973).

Two additional ambient vibration surveys were conducted in 1994, both while the building was damaged by the Northridge earthquake of January 17, 1994, and its aftershocks, and was not in use. The first survey took place on February 4 and 5, 1994, two and a half weeks after the earthquake. The second survey was conducted on April 19 and 20, 1994, three months after the Northridge earthquake, and one month following one of its larger aftershocks (20 March, 1994, M=5.2) (Trifunac et al. 1999a; Ivanović et al. 1999; 2000). The measured EW system frequencies were respectively 1.0 Hz and 1.1 Hz, and the NS system frequency was 1.4 Hz during both tests. The damage observed at the time of each experiment was photographed and documented (Trifunac et al. 1999b; Trifunac and Hao 2001). A significant change in the building, which can explain the higher measured system frequency during the second one of these two tests is that the building was restrained at the time of the second test. Wooden braces were installed to increase the structural capacity near the areas of structural damage (Figs. 2.4 and 2.5). Braces were placed in the first three or four stories at selected spans in the exterior longitudinal frames (A and D). Of all interior longitudinal frames, only the one at the first floor was restrained. There were no braces added to the transverse frames. We do not know when exactly the addition of the braces was completed, and whether there were braces at the time of the aftershock of March 20, 1994. However, we did observe that the width of the cracks increased (relative to our first inspection on February 4), especially of the shear cracks in the south (A) frame. We did not notice any new structural damage in the building or around its foundation. Figure 2.5 summarizes the location of structural damage and the braces as observed on April 19, 1994. The size of the "hinges" in Fig. 2.5 is proportional to the level of damage.

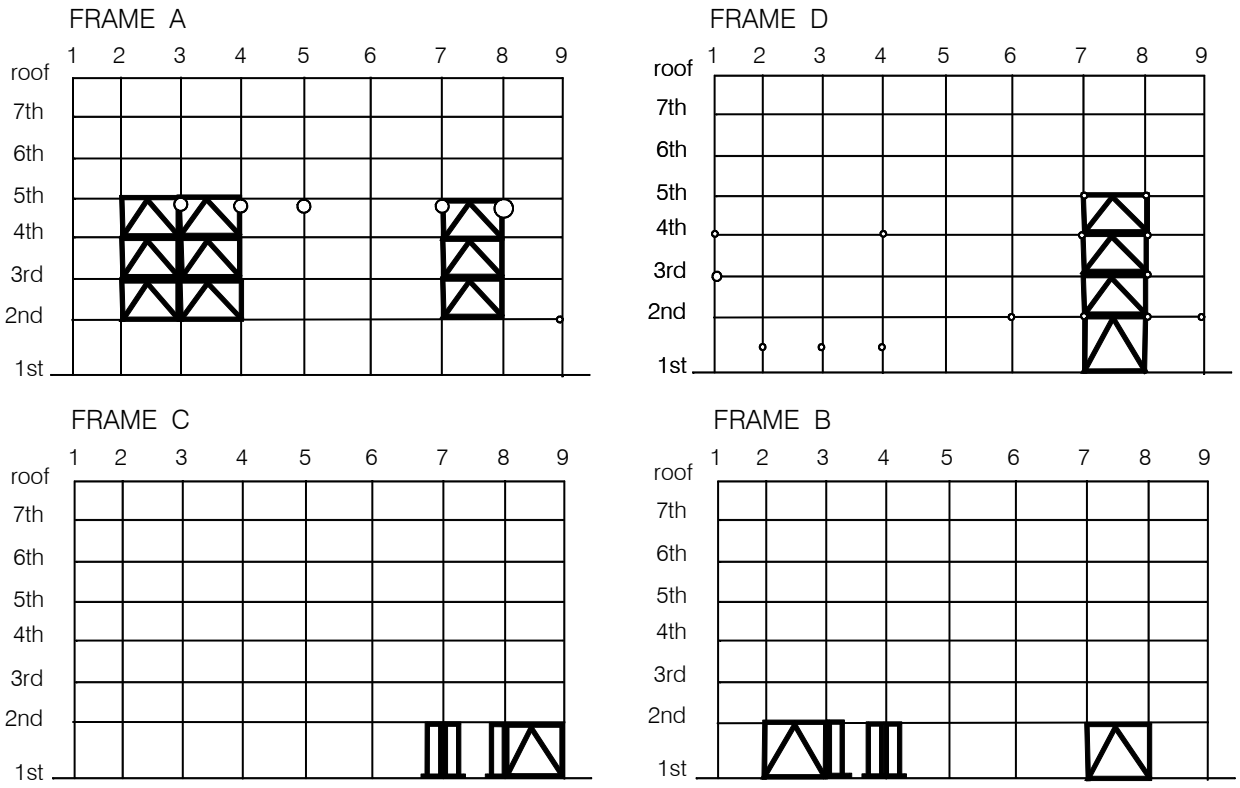

Fig. 2.5 Location of the braces, and schematic representation of the damage (shown by circles with size proportional to the damage) observed during the last ambient vibration experiment on 19 April, 1994.

2.2 Strong Motion Records

The first digitized strong motion records in the VN7SH building are those of the 1971 San Fernando earthquake, and the largest recorded motions are those of the 1994 Northridge earthquake. Figure 2.1 shows the location of the building relative to the faults of both of these earthquakes. It also shows the epicenters of two Northridge aftershocks, and the direction of wave arrival for other earthquakes for which records in this building are known to date and are cited in this work. All of these events are listed in Table 2.2. The earthquake magnitude, *M*, and epicentral distance, *R*, are also listed.

The building response to the 1971 San Fernando earthquake was recorded by three self-contained triaxial AR-240 accelerographs (Fig. 2.6a). These accelerograms were digitized manually, at a sampling rate > 50 samples per second (Trifunac and Lee 1973, Hudson et al., 1971; Trifunac et al., 1973). From the simplified sketch of the rupture history shown in Fig. 2.1 (Trifunac 1974), it is seen that the first strong motion waves arrived from N 22° E at depth about 9 to 13 km. The rupture propagated with velocity of about 2 km/s up and towards south, and the

last direct waves arrived 9 to 10 s later, from N 62° E. All the other earthquakes were recorded by a 13 channel CR-1 central recording system, and by one tri-axial SMA-1 accelerograph, with independent recording system, but with common trigger time with the CR-1 recorder. The locations of all the 16 channels are shown in Fig. 2.6b. On October 1, 1987, the Whittier-Narrows earthquake occurred. Before the 1992 Landers earthquake, one Whittier-Narrows aftershock and four smaller close by earthquakes were recorded. These records were used by Trifunac et al. (2001a,b) to study the time and amplitude dependent changes of the first EW and NS system frequencies.

The instrumentation in the VN7SH building is operated by the Strong Motion Instrumentation Program of the California Division of Mines and Geology (CDMG, currently the California Geological Survey). The records of events No. 2, 8, 9, 10 and 11 in Table 2.2 were digitized and released by CDMG. The records of events No. 3, 4, 5, 6, 7 and 12 were digitized at USC from Xerox copies in published reports (events 3–7) or from copies provided by the CDMG (event No. 12; Graizer, 1997). The LeAuto software package for automatic digitization of accelerograms and the LeBatch package for further processing of digitized data were used for this purpose (Trifunac and Lee 1979; Lee and Trifunac 1990). There were many other $M > 4$ aftershocks between the main event and December of 1994, but we do not know at this time if other aftershocks have been recorded in the building.

Table 2.2 Earthquakes recorded in the Van Nuys building for which digitized data are available

No.	Earthquake	Date	M	R [km]
1	San Fernando	02/09/1971	6.6	22
2	Whittier Narrows*	10/01/1987	5.9	41
3	Whitter-Narrows aft.	10/04/1987	5.3	38
4	Pasadena	10/03/1988	4.9	32
5	Montebello	06/12/1989	4.1	34
6	Malibu	01/19//1989	5.0	36
7	Sierra Madre	06/28/1991	5.8	44
8	Landers	06/28/1992	7.5	186
9	Big Bear	06/28/1992	6.5	149
10	Northridge	01/17/1994	6.5	1.5
11	Northridge aft.	03/20/1994	5.2	1.2
12	Northridge aft.	10/06/1994	4.5	10.8

*EW component of accelerograph on ground floor malfunctioned, and the record is not available. Hence this event is not included in the present analysis.

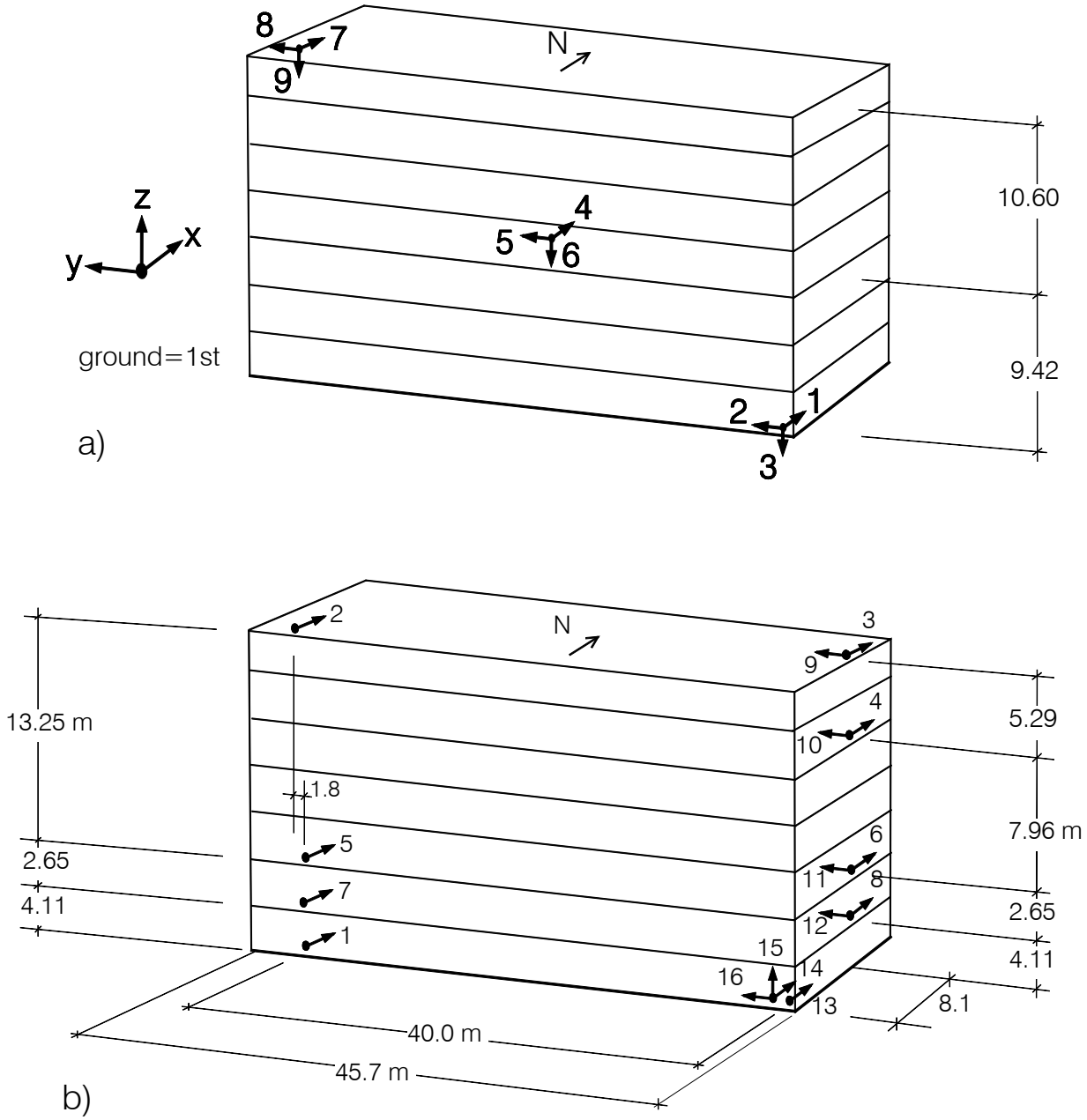

Fig. 2.6 Location of (a) the three AR-240 accelerographs, which recorded the San Fernando, 1971 earthquake, and of (b) the 13 channels of the CR-1 recording system, and the SMA-1 accelerograph (channels 14, 15, and 16), which recorded all earthquakes between mid 1970s and 1994.

3. METHODOLOGY

3.1 One-dimensional Continuous Wave Propagation Model of a Building

Long waves will "see" a bounded discrete medium such as a building as a "continuum." The simplest such model of a narrow building is a shear beam (Kanai 1965), and that of a long building is a shear plate (Todorovska et al. 1988; Todorovska and Trifunac 1989). If the mass and stiffness of the individual stories varies, then horizontally layered models, with piecewise continuous properties can be used, with interfaces at the floor slabs (Todorovska and Trifunac 1990; 2006a,b; Todorovska and Lee 1989; Şafak 1999). One such model is shown in Fig. 3.1.

An input wave at the base of the building will propagate upward and will be seen delayed and attenuated at observation points at different heights along the building. At the top, it will be reflected back, and will be seen delayed at consecutive observation points down towards the base. After hitting the base, it will be partially reflected and will again propagate upwards. After many such reflections, the motion resulting from constructive interference will dominate the response. Partial reflections will also occur at boundaries of impedance contrasts, as illustrated in Fig. 3.1.

The time delay between the motions at different stories can be observed by a naked eye in some earthquake records in tall buildings, but, to measure such delays, it is better to use some signal processing tool, the most common one being cross-correlation analysis. In this work we use deconvolution analysis (Snieder and Şafak 2006; Todorovska and Trifunac 2006c).

3.2 Impulse Response Computation

Let the building be a linear time-invariant system, with a single input – the ground motion, $u_{\text{ref}}(t)$, and multiple outputs – the story responses, $u_{\text{i}}(t)$ (Fig. 3.1). The input and outputs are related in the time domain by

$$\begin{aligned} u_i(t) &= (u_{\text{ref}} * h_i)(t) \\ &= \int_0^t u_{\text{ref}}(\tau)\, h_i(t-\tau)\, d\tau \end{aligned} \tag{3.1}$$

and in the frequency domain by

$$\hat{u}(\omega) = \hat{u}_{\text{ref}}(\omega)\, \hat{h}_i(\omega) \tag{3.2}$$

where $*$ indicates convolution, and the hat indicates Fourier transform. Function $h_i(t)$ is impulse response function, and represents the response at level i to input that is a Dirac delta function, $\delta(t)$

$$u_{\text{ref}}(t) = \delta(t) \quad \Leftrightarrow \quad u_i(t) = h_i(t) \tag{3.3}$$

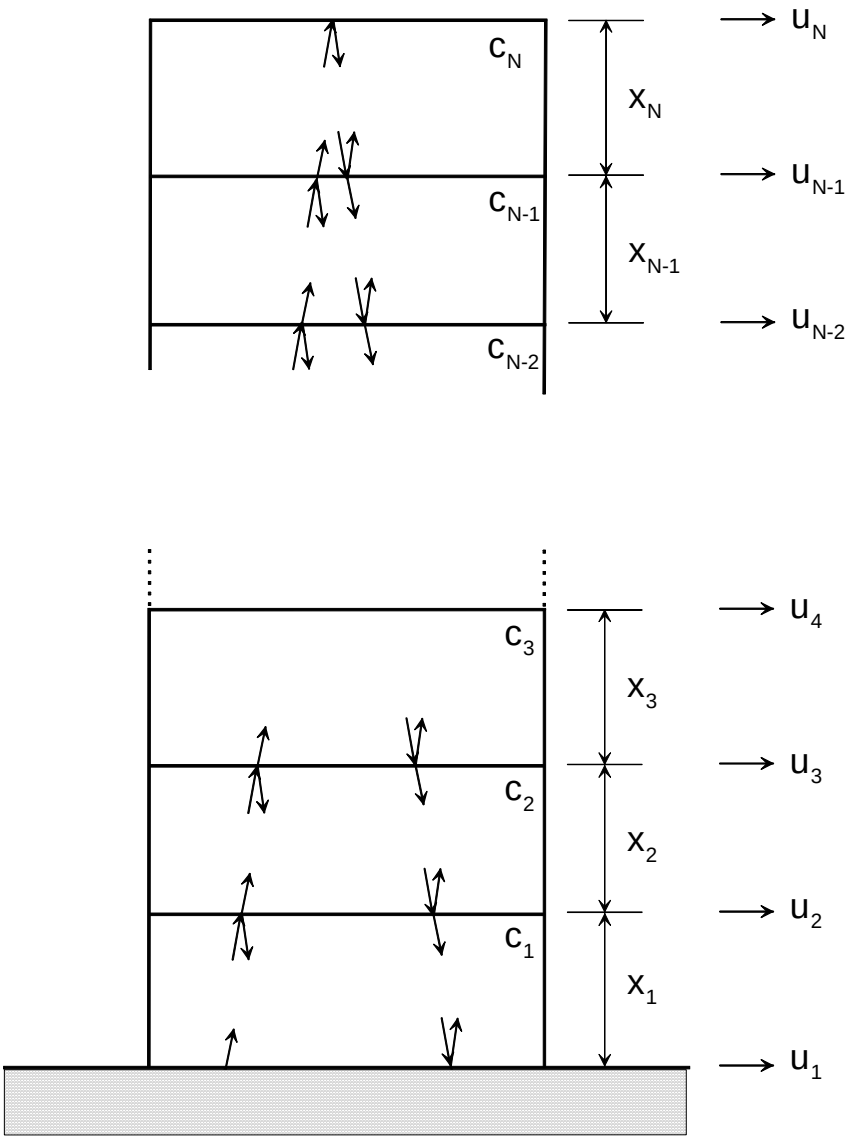

Fig. 3.1 An n-layer building model.

Function $\hat{h}_i(\omega)$ is the transfer function between the response at level i and the input, and represents the Fourier transform of the response to input such that $\hat{u}_{\text{ref}}(\omega) = 1$. The transfer function is the Fourier transform of the impulse response function

$$\hat{h}_i(\omega) = FT\{h_i(t)\} \tag{3.4}$$

The impulse response functions can be computed from any recorded response, by taking inverse Fourier transform of the corresponding transfer function, and can be used to simulate the propagation of a pulse through the building, using actual data. The time delays can be measured using these impulse response functions. We note here that the response at any level can be used as reference motion, in which case the impulse response function for that level would be a Delta-function.

The impulse response, $h_i(t)$, can be computed using

$$h_i(t) = FT^{-1}\left\{\frac{\hat{u}_i(\omega)\bar{\hat{u}}_{\text{ref}}(\omega)}{|\hat{u}_{\text{ref}}(\omega)| + \varepsilon}\right\} \tag{3.5}$$

where the bar indicates complex conjugate, and ε is a regularization parameter used to avoid singularities (Snieder and Şafak 2006). In this work, we used $\varepsilon = 0.1 * \bar{P}$ when u_{ref} is the ground floor record, and $\varepsilon = 0.05 * \bar{P}$ when u_{ref} is the roof record, where $\bar{P}$ is the average power of u_{ref}. Other optimization procedures can also be used to suppress noise in the deconvolution, e.g. such as the NIOM method used to analyze geotechnical borehole data (Haddadi and Kawakami 1998).

3.3 Damage Detection via Changes in Wave Travel Times

To identify changes in travel times, some reference travel times are needed to serve as baseline. For continuously monitored buildings, those could be values obtained from weak motion data recorded "immediately" before the earthquake, which could then be compared with values obtained from similar amplitude motions recorded after the earthquake. Using recorded strong motion data one can estimate "instantaneous" travel times from windowed data and track its changes versus time Todorovska and Trifunac 2006c). In this work we use strong motion data from earthquakes that damaged the building, and the time windows – before, during and after the occurrence of the major damage. The limits of these time intervals are chosen intuitively and when possible based on the results of other independent analyses. In each window, the

analysis will give the properties of an equivalent linear system representing the building in the corresponding time window.

3.4 Estimation of Fixed-Base Frequency via Wave Travel Times

Another significant product of the impulse response analysis is an estimate of the fundamental fixed-base frequency of vibration, using data from only two horizontal sensors, one at the point of fixity (ground level), and another one at the roof. In the following, we will assume the building response is predominantly one-dimensional (1D), the point of fixity is at ground level, and the deformations are mainly in shear. Then the fundamental *fixed-base* period of vibration T_1 of the building, modeled as a shear beam, is related to the wave travel time, τ_{tot}, it takes a wave to travel between the ground floor and roof

$$T_1 = 4\tau_{\text{tot}} \tag{3.6}$$

and the corresponding fundamental fixed-base frequency is $f_1 = 1/T_1$.

Snieder and Safak (2006) examined the effect of coupling with the soil on the estimate of f_1 using the impulse travel time. In their model, the building is a shear beam bonded to the soil, which is just another layer in 1D wave propagation problem through a layered medium. They proved that, for such a model, the travel time of the impulse is not affected by the coupling with the soil. Such a model is appropriate for anti-plane motions, and for in-plane motion by vertically incident waves and a building on a surface foundation. However, for the in-plane problem, buildings on rigid embedded foundations, or on surface rigid foundations and inclined wave incidence, not only deform but also move as a rigid body (translate and rotate). The motions of the upper floors due to the rigid body rocking cannot be separated from those due to deformation of the building even in the most ideal case of a relatively stiff base and floor slabs unless there are at least two vertical sensors at the base. Unfortunately, in the Van Nuys building there was only one vertical sensor at the ground floor. In this work, we assume that the contributions to the recorded motions we use to compute the impulse responses affects mostly the peak amplitude of the propagating pulse, while their effects on the shape of the pulse is small – hence on picking the pulse arrival time – are within the "noise" (i.e. errors due to all other simplifying assumptions).

Finally, we recall that the maximum concentrations of energy of the relative building response do not occur at the fixed-base frequencies of the building, f_1, but at the frequencies of the soil-structure system. The lowest such frequency, which is a result of the coupling of the soil

motion with the fundamental fixed-base frequency, we denote as f_{sys}, and we call it "first system frequency" or "the system frequency." The two frequencies are related by

$$f_{sys}^{-2} = f_1^{-2} + f_H^{-2} + f_R^{-2} \tag{3.7}$$

where f_H and f_R represent the horizontal and rocking frequencies of a rigid building on flexible soil. Eqn (3.6) implies that always $f_1 > f_{sys}$. In our previous work, we showed that was the case for the former Imperial County Services building (Todorovska and Trifunac 2006c), which is in favor of our hypothesis that f_1 we estimate from the impulse response analysis is approximately the fixed-base frequency. In this work, we further examine this hypothesis by checking that relationship for 11 events recorded by the Van Nuys building, and comparing the changes in f_1 from one even to another, and with time during different time intervals of the responses to the San Fernando and Northridge earthquakes. We also compare these changes with the observed damage.

4. RESULTS AND ANALYSIS

This chapter first presents plots of the impulse responses for 11 earthquakes, tabulated arrival and travel times between floors (as read from the impulse response plots), average shear wave velocities between floors, and normalized stiffness. Then results are presented for the fundamental fixed-base frequency, f_1, during the 11 earthquakes (as estimated from the wave travel times), and an analysis of its changes (as global indicators of damage) from one event to another and with time. The relation of f_1 to the soil structure system frequency, f_{sys}, during the 11 earthquakes and during five ambient vibration tests is also analyzed. This is followed by an analysis of the changes in the average wave velocity and stiffness of the floors between sensors (as local indicators of damage), and their relation to the observed degree, location, and time of occurrence of damage. Finally, some "force-displacement" relationships are presented involving f_1 and selected parameters of the excitation and of the response.

We consider only the EW (longitudinal) response, because it was less affected than the NS (transverse) response by torsion, and by rocking due to soil-structure interaction, and, consequently, has a better chance of being modeled satisfactorily by 1D wave propagation. Further, the observed damage appears to have been caused mainly by EW deformations. An analysis of the NS response would be more complex requiring simultaneous consideration of large rocking, coupled with torsion, and will be addressed in our future work.

4.1 Impulse Responses for EW Motions

The EW motions were recorded at the Ground floor (Channel 16), 2nd floor (Channel 12), 3-rd floor (Channel 11), 6th floor (Channel 10), and on the Roof (Channel 9) (Fig. 2.6b). Figures 4.1 through 4.11 show results for the impulse response functions at different levels of the building computed using eqn (3.5). The plots on the left hand side correspond to an input impulse at the ground floor, and those on the right hand side to an input impulse at the roof. The computed impulse response functions are shown only for the early stages of response to emphasize the arrival times of the primary pulses. The plots on the left show the input impulse at time $t = 0$ on the ground floor, which propagates up, arriving with some time delay at the upper floors, and then propagates down after being reflected from the roof. The input pulse has a finite width because of the effective windowing in time (due to finite duration of the record), and also due to the regularization parameter ε (we used $\varepsilon = 0.1$ for the case of an input impulse at the ground floor, and $\varepsilon = 0.05$ for the case of an input impulse at the roof). The plots on the right show the input impulse at time $t = 0$ at the roof, which then propagates down causally (in positive time), and also acausally (in negative time). The acausal wave corresponds to a wave propagating up in the physical model. For San Fernando, Landers and Northridge earthquakes,

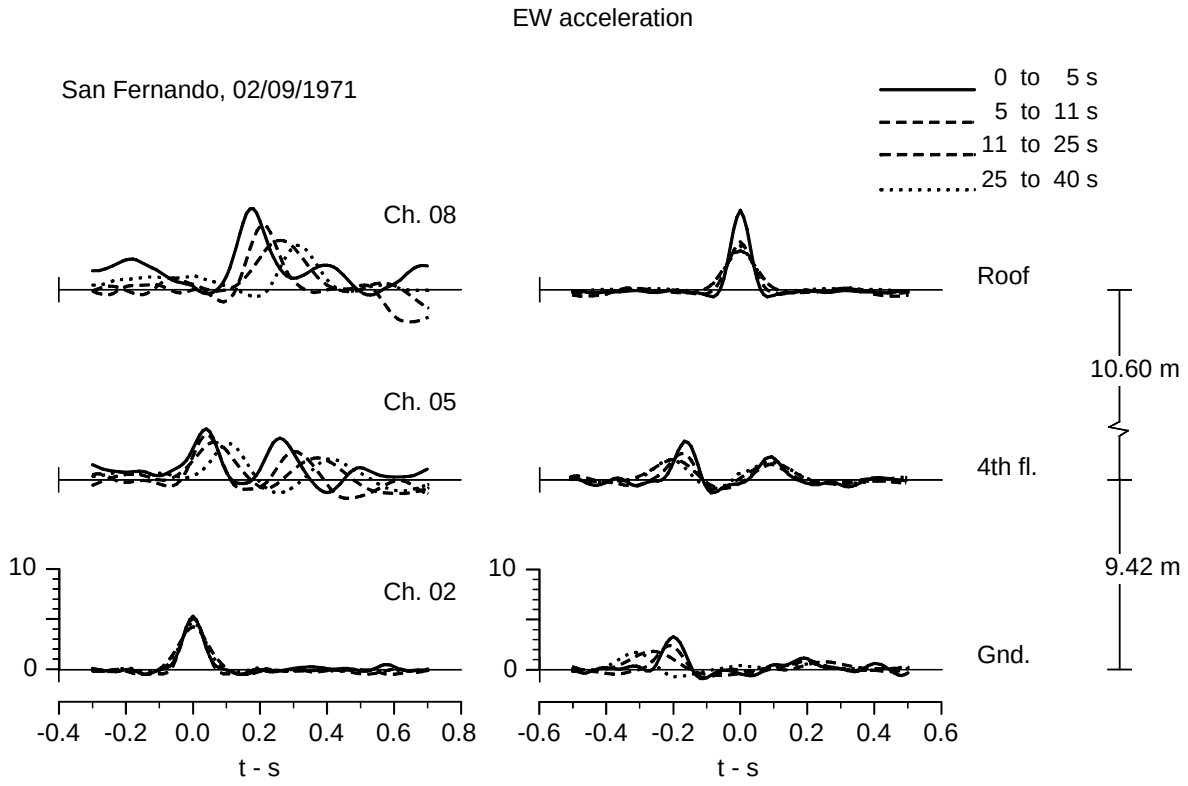

Fig. 4.1 Impulse response functions for EW motion of the Van Nuys building during the 1971 San Fernando earthquake.

which resulted in the largest excitations (see Figs 4.1, 4.7 and 4.9), the impulse responses were computed for different time windows, shown in the figures by different type of lines.

4.2 Readings of the Pulse Arrival Times, and Computed Wave Travel Times, Wave Velocities, and Fundamental Fixed-base Frequency

The pulse arrival times can be read most clearly for: (i) the direct wave going up – when the input impulse is at the base, and (ii) the direct acausal wave going down– when the input impulse is at the roof. In our analysis, we used the *mean* of the travel times estimated from these two pulses. The results of the readings of the arrival times for these two pulses are shown in Tables 4.1 through 4.11. The columns in these tables show: (1) the floor level, (2a) the arrival time t_i of the impulse at the particular floor, and (2b) the propagation time between the respective floors (sensors). Tables 4.12 through 4.22 show the mean of the two estimates of wave travel times between sensors, and the inferred wave speeds. The first two columns in Tables 4.12 through

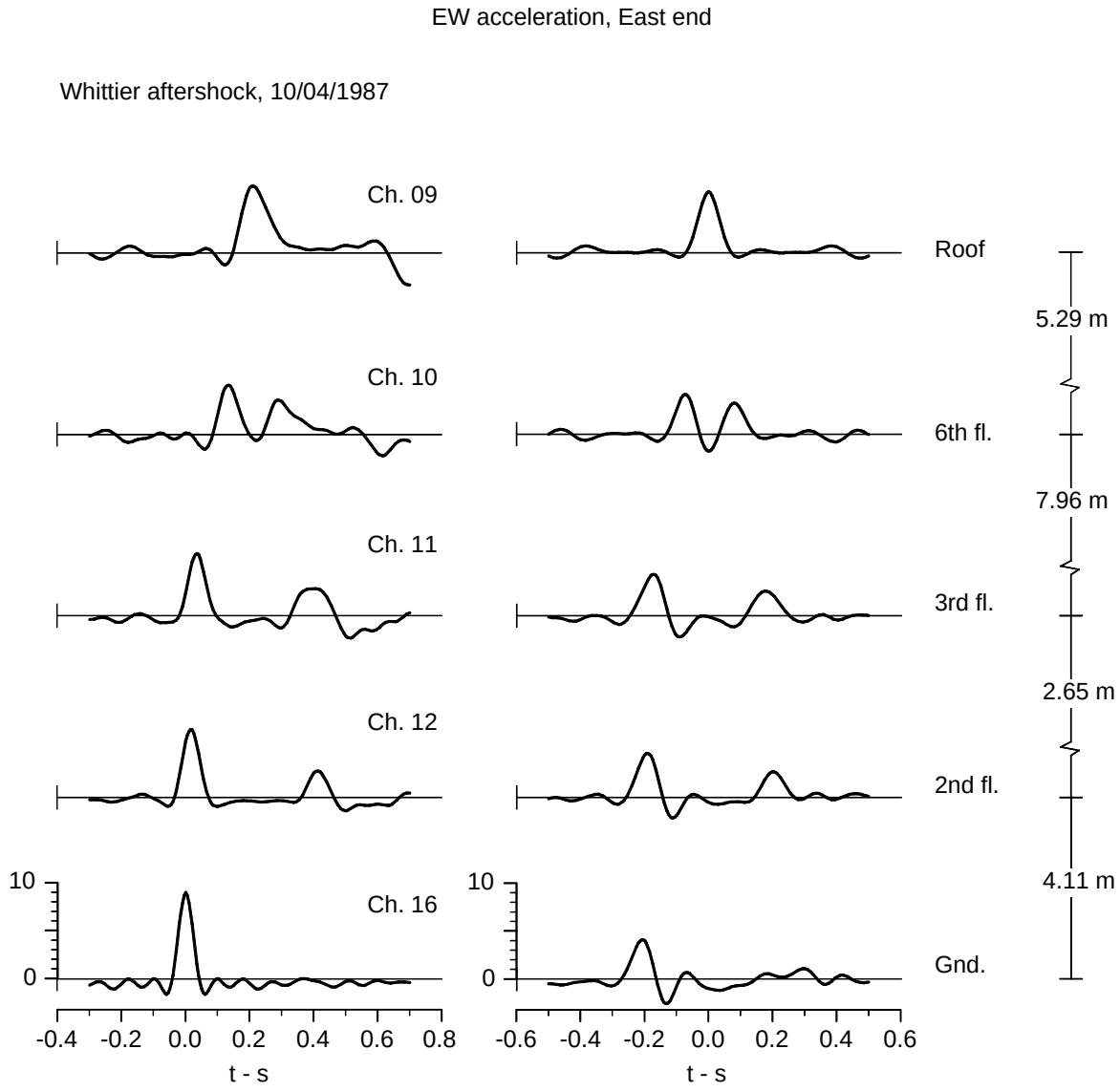

Fig. 4.2 Same as Fig. 4.1 but for the aftershock of the 1987 Whittier Narrows earthquake.

4.22 show: (1) the floor level, and (2) the distance between sensors, h_i (in meters). The following group of columns shows: (3a) the mean travel time τ_i, and (3b) the average velocity of wave propagation between sensors, $v_i = h_i / \tau_i$ (over one or several floors within segment i, see Fig. 3.1). For the San Fernando, Landers and Northridge earthquakes (Tables 4.12, 4.18 and 4.20), such results are shown for each time segment, and the changes of v_i and shear moduli μ_i with respect to the initial time intervals, used as baseline data, are shown in additional columns.

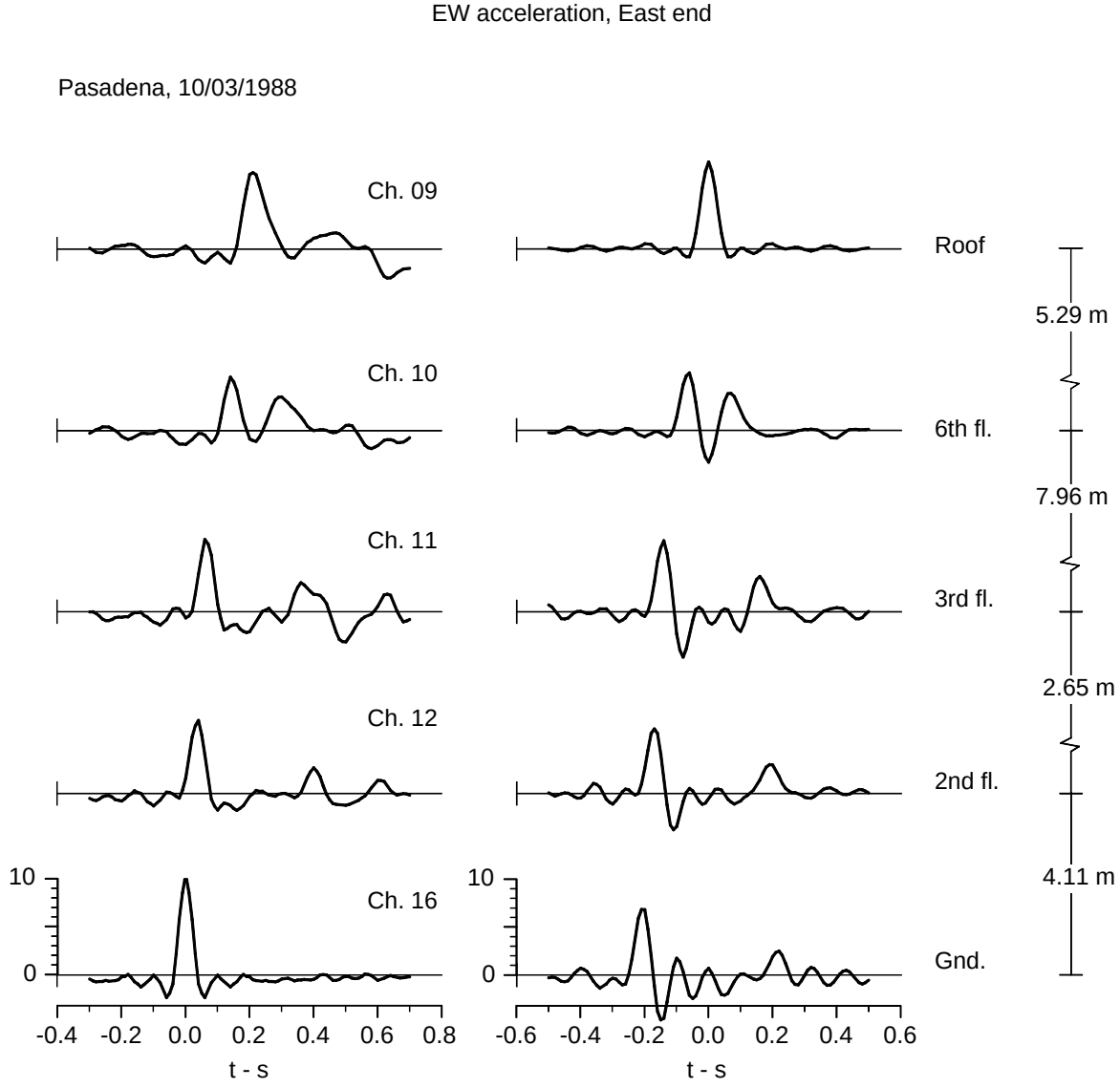

Fig. 4.3 Same as Fig. 4.1 but for the 1988 Pasadena earthquake.

The change in velocities can be computed from the travel times as $\Delta v_i / v_{\text{ref}} = \left(v_i - v_{\text{ref}}\right) / v_{\text{ref}} = \tau_{\text{ref}} / \tau_i - 1$. The change of rigidity was estimated based on the fact that, for almost uniform distribution of density along the height of the building, $\mu_i \sim v_i^2$, where μ_i is the shear modulus for segment i of the building. Then $\Delta \mu_i / \mu_{\text{ref}} = \left(\tau_{\text{ref}} / \tau_i\right)^2 - 1$.

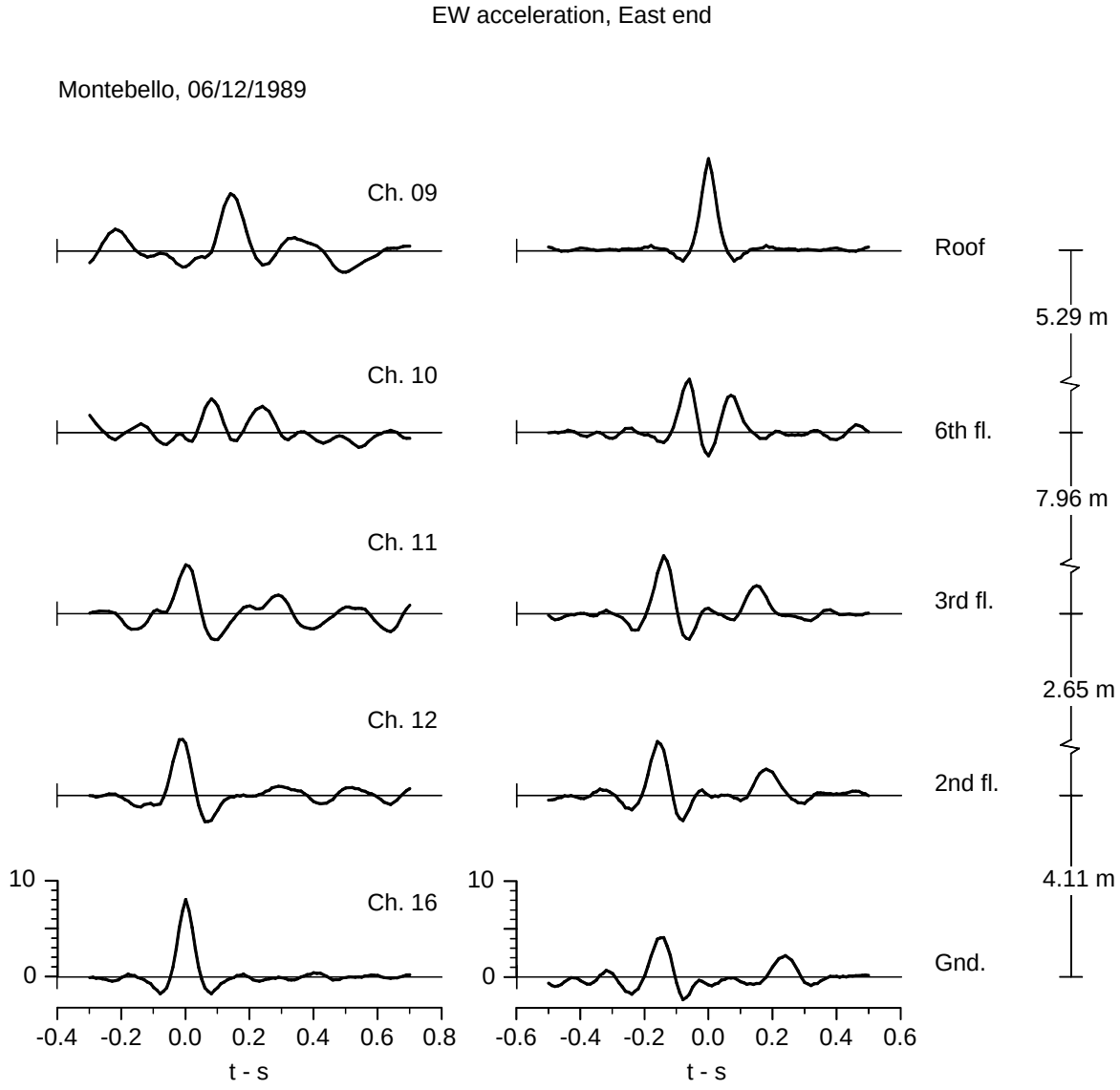

Fig. 4.4 Same as Fig. 4.1 but for the 1989 Montebello earthquake.

Finally, Table 4.23 shows, for all of the events, the (mean) *total* travel times along the height of the building, τ_{tot}, and the corresponding estimates of the shear wave velocity of an equivalent uniform shear beam, v_{eq}, and the fundamental fixed-base frequency, f_1 (see Section 3.4). For the San Fernando, Landers and Northridge earthquakes, results are also shown for each of the time intervals (i.e. record segments) analyzed, and the percentage changes in wave velocity and in shear moduli, relative to the respective initial time interval. Columns (1a) and (1b) show the earthquake name and date. Columns (1c) and (1d) show the two letter code assigned

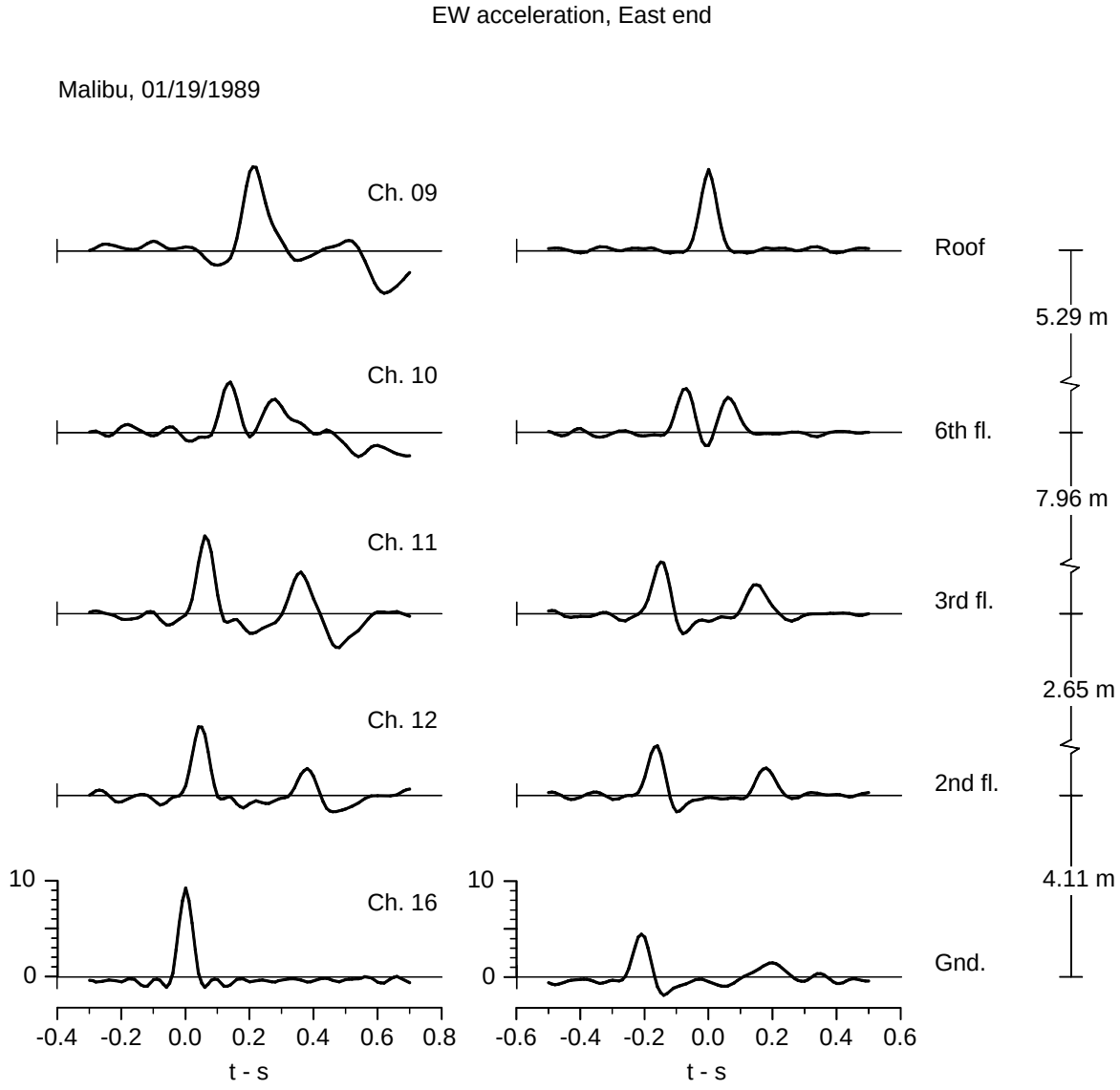

Fig. 4.5 Same as Fig. 4.1 but for the 1989 Malibu earthquake.

to the particular event or its segment, and the time limits for the corresponding record/segment used in the analysis. Columns (2a), (2b) and (2c) show τ_{tot}, v_{eq} and f_1. Finally, for the events for which data from multiple segments were analyzed, columns (2d) and (2e) show the percentage changes of f_1, and of the shear moduli, relative to the respective initial segment.

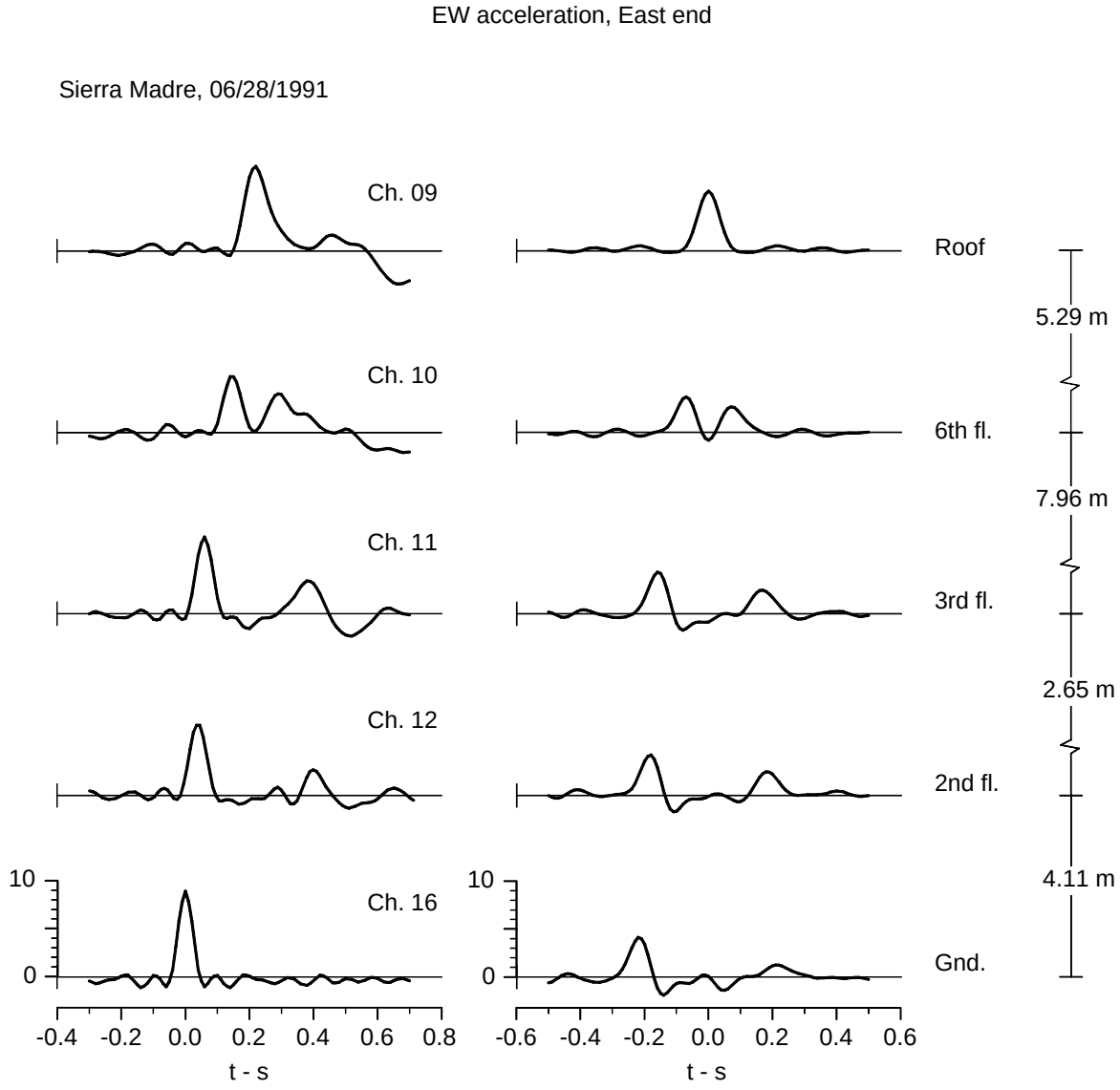

Fig. 4.6 Same as Fig. 4.1 but for the 1991 Sierra Madre earthquake.

Some basic parameters of the recorded motions during each earthquake/segment are shown in Table 2.24. Columns (1) and (2) show the code identifying the event/segment (see Table 2.23), and the corresponding estimate of f_1. Columns (3a), (3b), (3c) and (3d) show respectively the peak ground acceleration $a_{\max}^{\text{Gnd}}$, peak roof acceleration $a_{\max}^{\text{Roof}}$, peak ground velocity $v_{\max}^{\text{Gnd}}$, and the peak roof relative displacement $d_{\max}$. Columns (3e), (3f), (3g) and (3h) show some quantities derived from the values shown in the preceding columns, in particular,

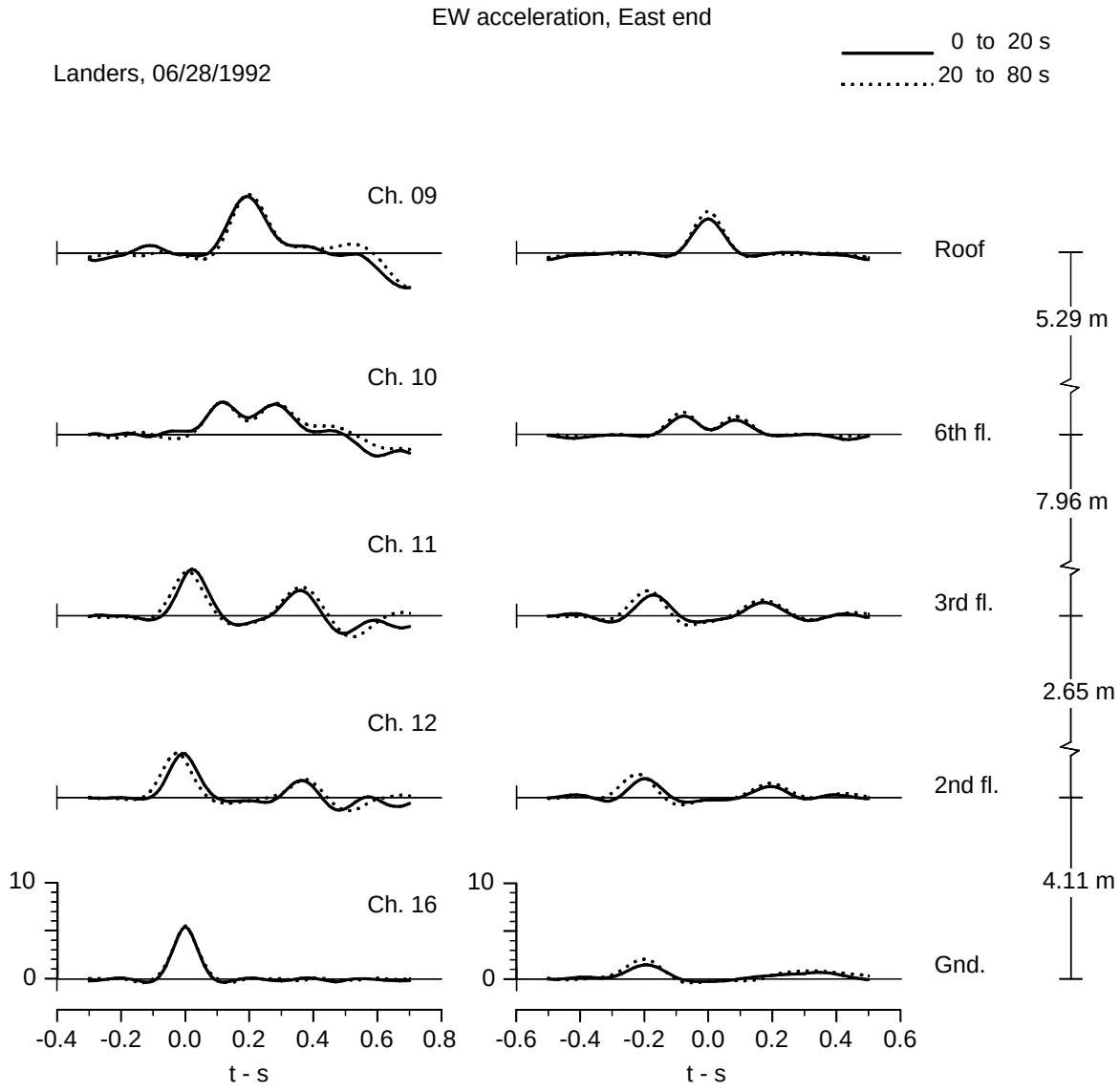

Fig. 4.7 Same as Fig. 4.1 but for the 1992 Landers earthquake.

they show the average value of the ground and roof peak acceleration $\bar{a}_{\max} = \left(a_{\max}^{\text{Gnd}} + a_{\max}^{\text{Roof}}\right)/2$, $d_{\max}\omega_1^2$, f_1^2 and $v_{\max}^{\text{Gnd}}/(4f_1)$.

The following sections show graphically results for the estimated wave velocities, changes in wave velocities and shear moduli, and fixed-base frequency, and present an analysis of the observed changes. We first analyze the global properties (the fixed-base frequency f_1), and

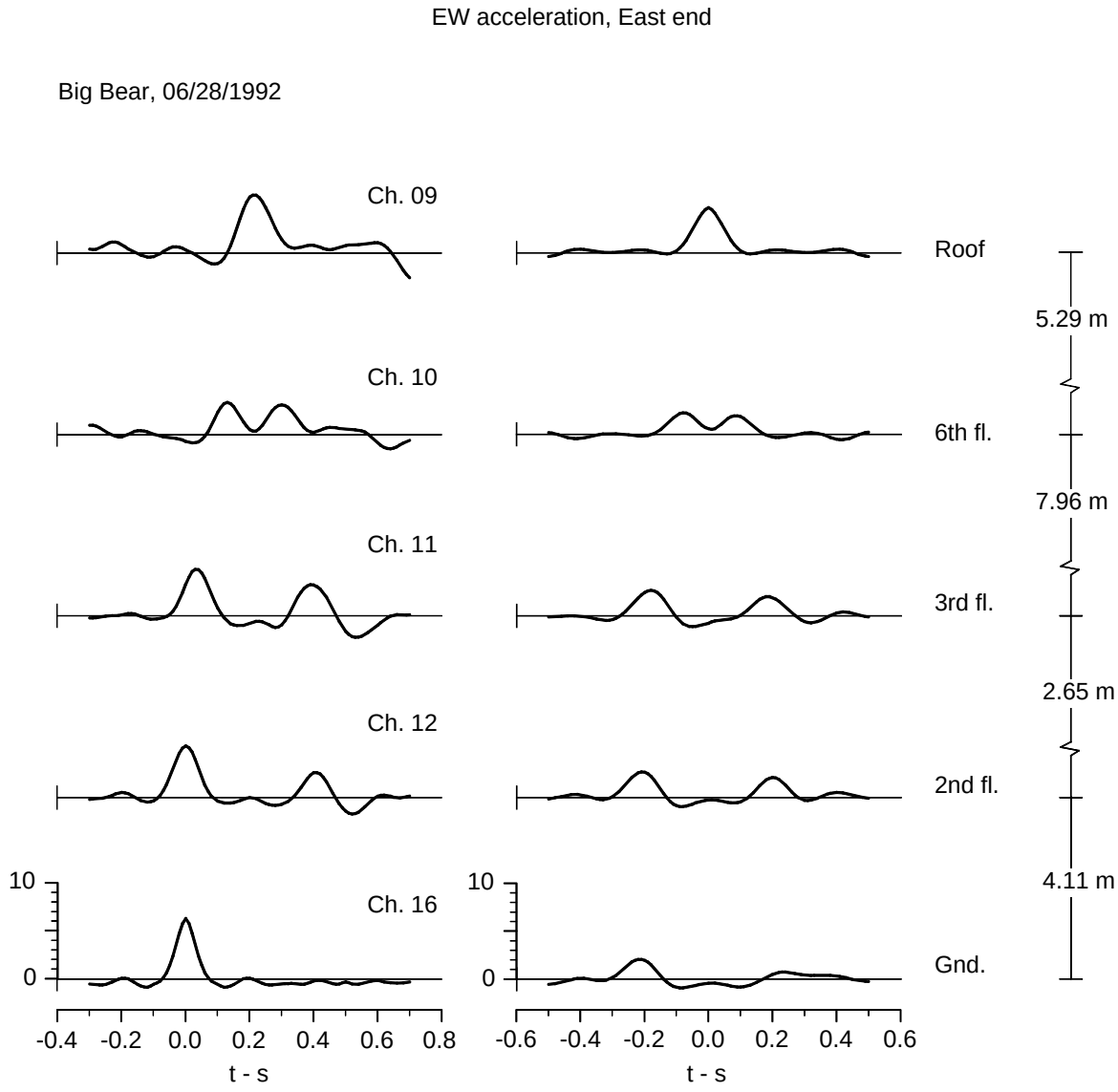

Fig. 4.8 Same as Fig. 4.1 but for the 1992 Big Bear earthquake.

then proceed with an analysis of the local properties (average floor velocities and stiffness), as they changed over a period of almost 24 years (between February 1971 and December 1994).

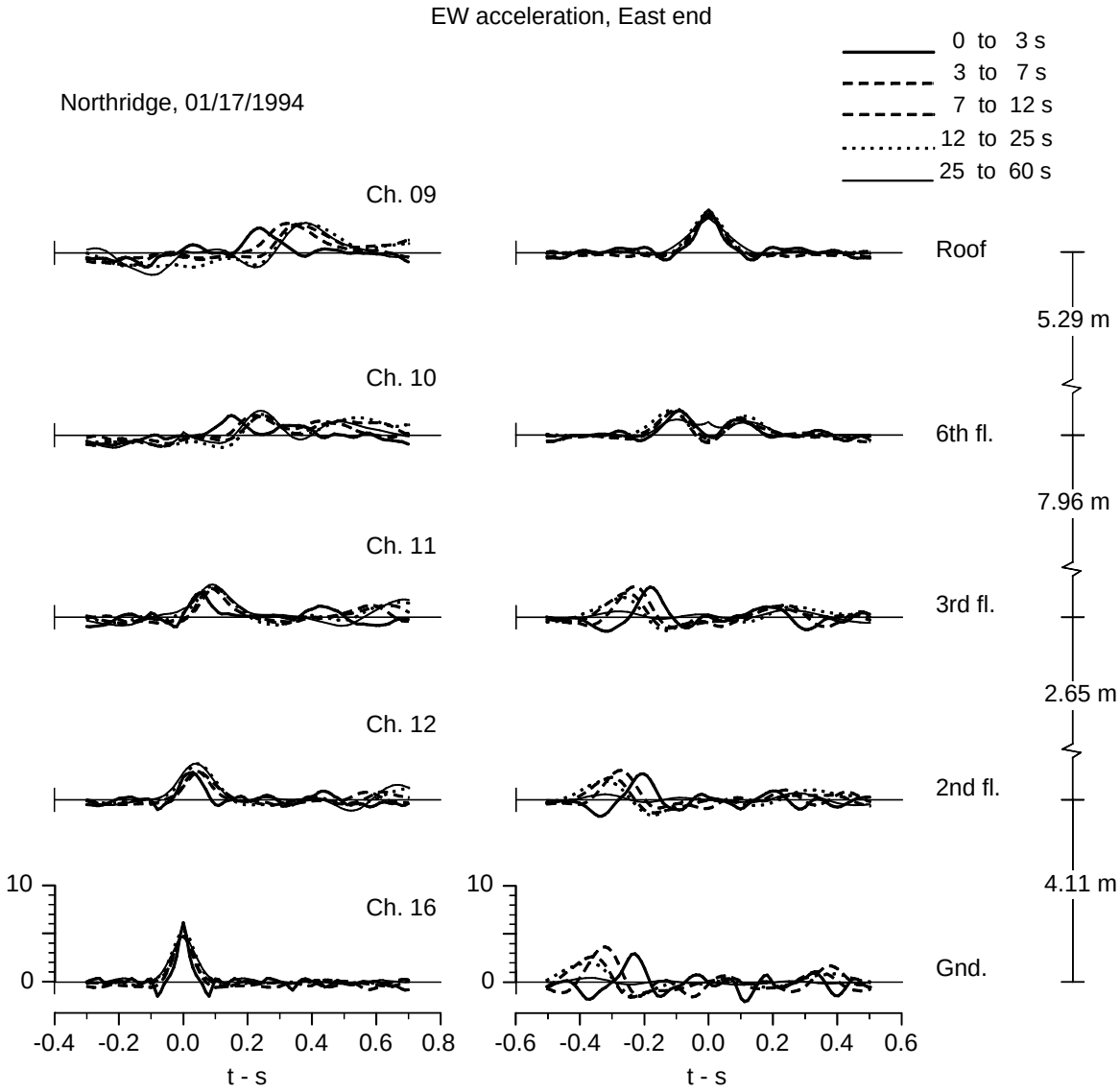

Fig. 4.9 Same as Fig. 4.1 but for the 1994 Northridge earthquake.

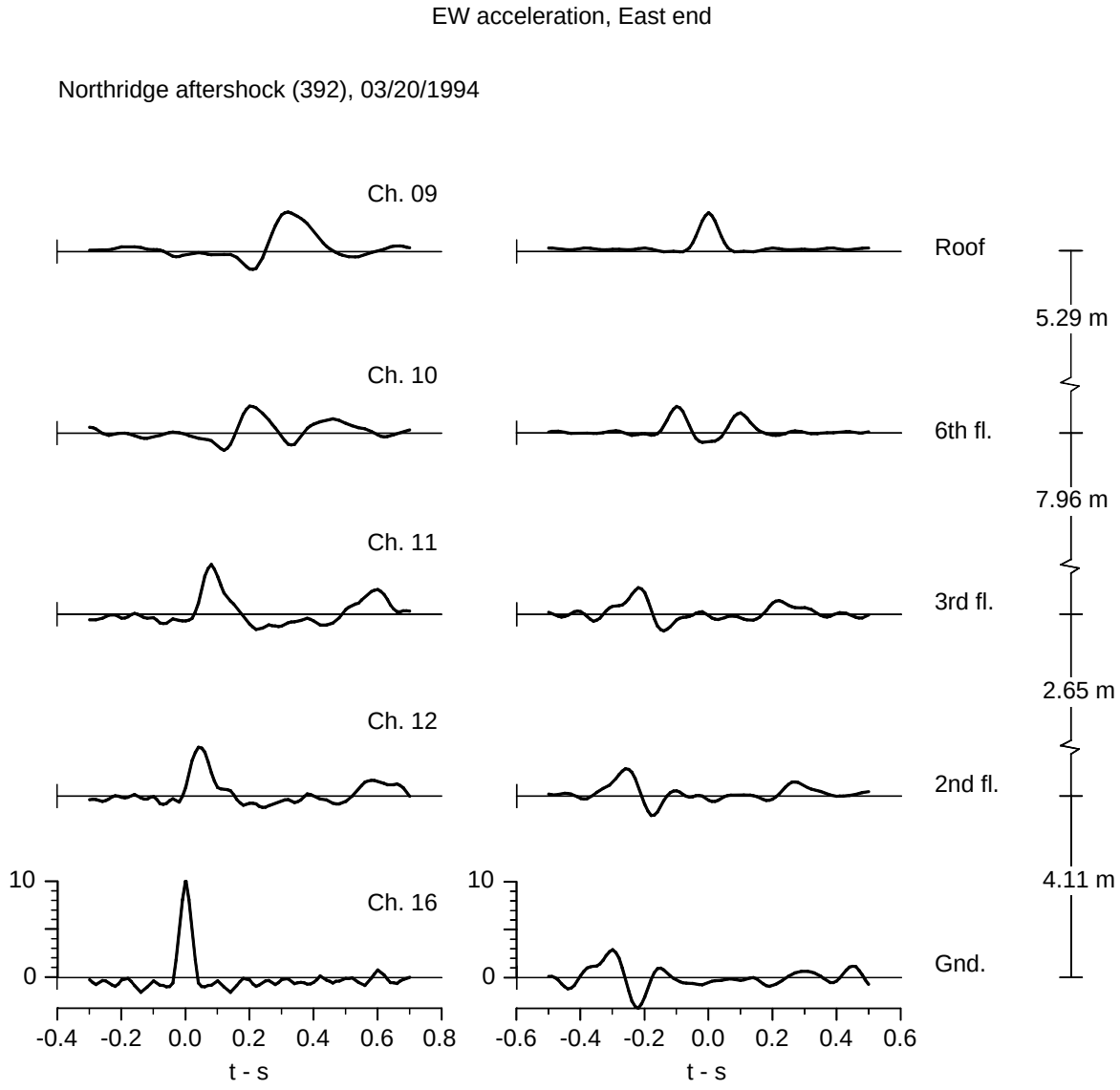

Fig. 4.10 Same as Fig. 4.1 but for the March 27, 1994, aftershock of the Northridge earthquake.

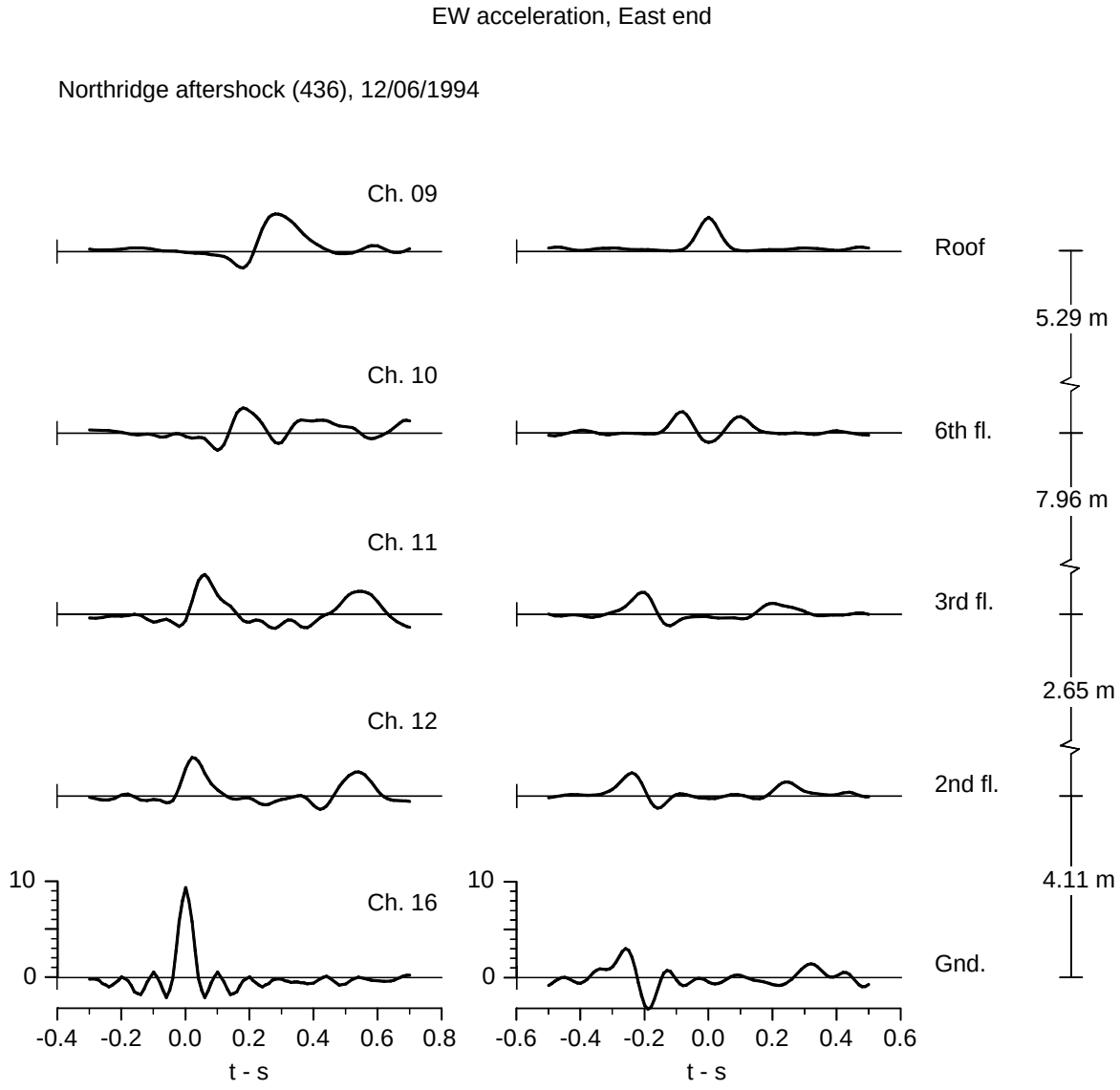

Fig. 4.11 Same as Fig. 4.1 but for the December 6, 1994, aftershock of the Northridge earthquake.

Table 4.1 San Fernando, 1971, EW motions: measured pulse arrival times, t_i, and corresponding wave travel times, τ_i

		EW Motions							
		t < 5s		5 < t < 11s		11 < t < 25s		25 < t < 40s	
Input Impulse	(1)	(2a)	(2b)	(3a)	(3b)	(4a)	(4b)	5(a)	(5b)
	Floor	t_i - s	τ_i - s	t - s	τ_i - s	t_i - s	τ_i - s	t_i - s	τ_i - s
Gound floor, pulse going up	Roof	0.175		0.205		0.255		0.305	
			0.105		0.130		0.165		0.170
	4th	0.070		0.075		0.090		0.135	
			0.070		0.075		0.090		0.135
	Ground	0		0		0		0	
Roof, ausal pulse going down	Roof	0		0		0		0	
			0.125		0.133		0.150		0.160
	4^{th}	0.125		0.133		0.150		0.160	
			0.070		0.067		0.105		0.145
	Ground	0.195		0.200		0.255		0.305	

Table 4.2. Same as Table 4.1 but for Whittier Aftershock, 1987

		EW Motions	
		t < 24 s	
	(1)	(2a)	(2b)
Input Impulse	Floor	t_i - s	τ_i - s
Ground floor, pulse going up	Roof	0.210	
			0.075
	6^{th}	0.135	
			0.100
	3^{rd}	0.035	
			0.020
	2^{nd}	0.015	
			0.015
	Ground	0	
Roof, acausal pulse going down	Roof	0	
			0.077
	6^{th}	0.077	
			0.095
	3^{rd}	0.172	
			0.025
	2^{nd}	0.197	
			0.008
	Ground	0.205	

Table 4.3. Same as Table 4.1 but for Pasadena earthquake, 1988

		EW Motions	
		t < 24.5 s	
	(1)	(2a)	(2b)
Input Impulse	Floor	t_i - s	τ_i - s
Ground floor, pulse going up	Roof	0.210	
			0.065
	6th	0.145	
			0.080
	3rd	0.065	
			0.030
	2nd	0.035	
			0.035
	Ground	0	
Roof, acausal pulse going down	Roof	0	
			0.065
	6th	0.065	
			0.088
	3rd	0.153	
			0.027
	2nd	0.180	
			0.020
	Ground	0.200	

Table 4.4. Same as Table 4.1 but for Malibu earthquake, 1989

		EW Motions	
		t < 25s	
	(1)	(2a)	(2b)
Input Impulse	Floor	t_i - s	τ_i - s
Ground floor, pulse going up	Roof	0.215	
			0.080
	6th	0.135	
			0.075
	3rd	0.060	
			0.025
	2nd	0.035	
			0.035
	Ground	0	
Roof, acausal pulse going down	Roof	0	
			0.065
	6th	0.065	
			0.082
	3rd	0.147	
			0.025
	2nd	0.172	
			0.031
	Ground	0.203	

Table 4.5. Same as Table 4.1 but for Montebello earthquake, 1989

		EW Motions	
		t < 24s	
	(1)	(2a)	(2b)
Input Impulse	Floor	t_i - s	τ_i - s
Ground floor, pulse going up	Roof	0.190	
			0.067
	6th	0.123	
			0.080
	3rd	0.043	
			0.009
	2nd	0.034	
			0.034
	Ground	0	
Roof, acausal pulse going down	Roof	0	
			0.067
	6th	0.067	
			0.078
	3rd	0.145	
			0.022
	2nd	0.167	
			0.028
	Ground	0.195	

Table 4.6. Same as Table 4.1 but for Sierra Madre earthquake, 1991

		EW Motions	
		t < 23s	
	(1)	(2a)	(2b)
Input Impulse	Floor	t_i - s	τ_i - s
Ground floor, pulse going up	Roof	0.220	
			0.075
	6th	0.145	
			0.085
	3rd	0.060	
			0.020
	2nd	0.040	
			0.040
	Ground	0	
Roof, acausal pulse going down	Roof	0	
			0.070
	6th	0.070	
			0.092
	3rd	0.162	
			0.020
	2nd	0.182	
			0.033
	Ground	0.215	

Table 4.7. Same as Table 4.1 but for Landers earthquake, 1992

		EW Motions			
		t < 20s		20 < t < 80s	
	(1)	(2a)	(2b)	(3a)	(3b)
Input Impulse	Floor	t_i - s	τ_i - s	t - s	τ_i - s
Ground floor, pulse going up	Roof	0.195		0.200	
			0.085		0.090
	6th	0.110		0.110	
			0.085		0.090
	3rd	0.025		0.020	
			0.020		0.015
	2nd	0.005		0.005	
			0.005		0.005
	Ground	0		0	
Roof, acausal pulse going down	Roof	0		0	
			0.080		0.085
	6th	0.080		0.085	
			0.090		0.100
	3rd	0.170		0.185	
			0.025		0.020
	2nd	0.195		0.205	
			0.005		0.005
	Ground	0.200		0.210	

Table 4.8. Same as Table 4.1 but for Big Bear earthquake, 1992

		EW Motions	
		t < 40s	
	(1)	(2a)	(2b)
Input Impulse	Floor	t_i - s	τ_i - s
Ground floor, pulse going up	Roof	0.215	
			0.085
	6th	0.130	
			0.095
	3rd	0.035	
			0.030
	2nd	0.005	
			0.005
	Ground	0	
Roof, acausal pulse going down	Roof	0	
			0.080
	6th	0.080	
			0.100
	3rd	0.180	
			0.025
	2nd	0.205	
			0.005
	Ground	0.215	

Table 4.9. Same as Table 4.1 but for Northridge earthquake, 1994

		EW Motions									
		t < 5s		3 < t < 7s		7 < t > 12s		12 < t < 25s		25 < t < 60s	
	(1)	(2a)	(2b)	(3a)	(3b)	(4a)	(4b)	(5a)	(5b)	(6a)	(6b)
Input Impulse	Floor	t_i - s	. τ_i- s	t - s	. τ_i- s	t_i - s	. τ_i- s	t_i - s	. τ_i- s	t_i - s	. τ_i- s
Ground floor, pulse going up	Roof	0.300		0.325		0.365		0.375		0.375	
			0.095		0.105		0.120		0.125		0.125
	6th	0.205		0.220		0.245		0.250		0.750	
			0.130		0.135		0.150		0.150		0.150
	3rd	0.075		0.085		0.095		0.100		0.100	
			0.040		0.040		0.050		0.050		0.050
	2nd	0.035		0.045		0.045		0.050		0.050	
			0.035		0.045		0.045		0.050		0.050
	Ground	0		0		0		0		0	
Roof, acausal pulse going down	Roof	0		0		0		0		0	
			0.090		0.095		0.100		0.115		0.115
	6th	0.090		0.095		0.100		0.115		0.115	
			0.115		0.135		0.155		0.150		0.150
	3rd	0.205		0.230		0.255		0.265		0.265	
			0.050		0.040		0.050		0.060		0.060
	2nd	0.255		0.275?		0.305?		0.325		0.325	
			0.035		0.050		0.055		0.060		0.060
	Ground	0.290		0.325?		0.306?		0.385		0.385	

Table 4.10. Same as Table 4.1 but for Northridge Aftershock, March 1994

		EW Motions	
		t < 26s	
	(1)	(2a)	(2b)
Input Impulse	Floor	t_i - s	τ_i - s
Ground floor, pulse going up	Roof	0.320	
			0.115
	6th	0.205	
			0.125
	3rd	0.080	
			0.035
	2nd	0.045	
			0.045
	Ground	0	
Roof, acausal pulse going down	Roof	0	
			0.100
	6th	0.100	
			0.115
	3rd	0.215	
			0.045
	2nd	0.260	
			0.040
	Ground	0.300	

Table4.11. Same as Table 4.1 but for Northridge aftershock, December 1994

		EW Motions	
		t < 26s	
	(1)	(2a)	(2b)
Input Impulse	Floor	t_i - s	τ_i - s
Ground floor, pulse going up	Roof	0.280	
			0.100
	6th	0.180	
			0.120
	3rd	0.060	
			0.035
	2nd	0.025	
			0.025
	Ground	0	
Roof, acausal pulse going down	Roof	0	
			0.090
	6th	0.090	
			0.112
	3rd	0.202	
			0.038
	2nd	0.240	
			0.020
	Ground	0.260	

Table 4.12 San Fernando, 1971, EW motions: mean travel times, τ_i (over the two measurements; see top and bottom parts of Table 4.1), and average wave velocities for the segments of the building between sensors, ν_i. For the subsequent time intervals, the percent changes in wave velocities and corresponding rigidities are also shown (relative to the initial time interval, t < 5 s).

		EW Motions													
		t < 5 s		5 < t < 11 s				11 < t < 25 s				25 < t < 40 s			
(1)	(2)	(3a)	(3b)	(4a)	(4b)	(4c)	(4d)	(5a)	(5b)	(5c)	(5d)	(6a)	(6b)	(6c)	(6d)
Floor	h_i - m	τ_i - s (mean)	ν_i / ν_{ref}	τ_i - s (mean)	ν_i - m/s	$\Delta \nu_i / \nu_{ref}$ %	$\Delta\mu_i/\mu_{ref}$ %	τ_i - s (mean)	ν_i - m/s	$\Delta \nu_i / \nu_{ref}$ %	$\Delta\mu_i/\mu_{ref}$ %	τ_i - s (mean)	ν_i - m/s	$\Delta \nu_i / \nu_{ref}$ %	$\Delta\mu_i/\mu_{ref}$ %
Roof															
	10.60	0.115	92.2	0.133	79.7	-13.5	-25.2	0.150	70.7	-23.3	-41.2	0.160	66.3	-28.1	-48.3
4th															
	9.42	0.070	134.60	0.1	134.60	0.0	0.0	0.1	89.70	-33.4	-55.6	0.1	65.00	-51.7	-76.7
Ground															

Table 4.13 Same as Table 4.12 but for Whittier Aftershock, 1987

		EW Motions	
		t < 24 s	
(1)	(2)	(3a)	(3b)
Floor	h_i - m	τ_i - s (mean)	ν_i - m/s
Roof			
	5.29	0.076	69.60
6^{th}			
	7.95	0.097	81.96
3^{rd}			
	2.65	0.022	120.45
2^{nd}			
	4.11	0.011	373.64
Ground			

Table 4.14. Same as Table 4.12 but for Pasadena earthquake, 1988

		EW Motions	
		t < ??? s	
(1)	(2)	(3a)	(3b)
Floor	h_i - m	τ_i - s (mean)	ν_i - m/s
Roof			
	5.29	0.065	81.38
6th			
	7.95	0.084	94.64
3rd			
	2.65	0.028	94.64
2nd			
	4.11	0.028	146.78
Ground			

Table 4.15 Same as Table 4.12 but for Malibu earthquake, 1989.

		EW Motions	
		t < 25 s	
(1)	(2)	(3a)	(3b)
Floor	h_i - m	τ_i - s (mean)	ν_i - m/s
Roof			
	5.29	0.072	73.47
6th			
	7.95	0.078	101.92
3rd			
	2.65	0.025	106.00
2nd			
	4.11	0.033	124.55
Ground			

Table 4.16 Same as Table 4.12 but for Montebello earthquake, 1989

		EW Motions	
		t < 24 s	
(1)	(2)	(3a)	(3b)
Floor	h_i - m	τ_i - s (mean)	ν_i - m/s
Roof			
	5.29	0.067	78.96
6th			
	7.95	0.079	100.63
3rd			
	2.65	0.016	165.63
2nd			
	4.11	0.031	132.58
Ground			

Table 4.17 Same as Table 4.12 but for Sierra Madre earthquake, 1991

		EW Motions	
		t < 23 s	
(1)	(2)	(3a)	(3b)
Floor	h_i - m	τ_i - s (mean)	ν_i - m/s
Roof			
	5.29	0.072	73.47
6th			
	7.95	0.088	90.34
3rd			
	2.65	0.020	132.50
2nd			
	4.11	0.036	114.17
Ground			

Table 4.18 Same as Table 4.12 but for Landers earthquake, 1992

		EW Motions					
		t < 20 s		20 < t < 80 s			
(1)	(2)	(3a)	(3b)	(4a)	(4b)	(4c)	(4d)
Floor	h_i - m	τ_i - s (mean)	ν_i - m/s	τ_i - s (mean)	ν_i - m/s	$\Delta\nu_i / \nu_{ref}$ %	$\Delta\mu_i/\mu_{ref}$ %
Roof							
	5.29	0.082	64.51	0.087	60.80	-5.80	-11.2
6th							
	7.95	0.087	91.38	0.095	83.68	-8.40	-16.1
3rd							
	2.65	0.022	120.45	0.017	155.88	?	?
2nd							
	4.11	0.005	822.00	0.005	822.00	?	?
Ground							

Table 4.19 Same as Table 4.12 but for Big Bear earthquake, 1992

		EW Motions	
		t < 40 s	
(1)	(2)	(3a)	(3b)
Floor	h_i - m	τ_i - s (mean)	ν_i - m/s
Roof			
	5.29	0.082	64.51
6th			
	7.95	0.098	81.12
3rd			
	2.65	0.027	98.15
2nd			
	4.11	0.005	822.00
Ground			

Table 4.20 Same as Table 4.12 but for Northridge earthquake, 1994

		EW Motions																	
		t < 5 s		3 < t < 7 s				7 < t > 12 s				12 < t < 25 s				25 < t < 60 s			
(1)	(2)	(3a)	(3b)	(4a)	(4b)	(4c)	(4d)	(5a)	(5b)	(5c)	(5d)	(6a)	(6b)	(6c)	(6d)	(7a)	(7b)	(7c)	(7d)
Floor	h_i - m	τ_i - s (mean)	v_i - m/s	τ_i - s (mean)	v_i - m/s	$\Delta v_i / v_{ref}$ %	$\Delta\mu_i/\mu_{ref}$ %	τ_i - s (mean)	v_i - m/s	$\Delta v_i / v_{ref}$ %	$\Delta\mu_i/\mu_{ref}$ %	τ_i - s (mean)	v_i - m/s	$\Delta v_i / v_{ref}$ %	$\Delta\mu_i/\mu_{ref}$ %	τ_i - s (mean)	v_i - m/s	$\Delta v_i / v_{ref}$ %	$\Delta\mu_i/\mu_{ref}$ %
Roof																			
	5.29	0.092	57.5	0.100	52.9	-8.0	-15.4	0.110	48.1	-16.4	-30.0	0.120	44.1	-23.3	-41.3	0.120	44.1	-23.3	41.2
6th																			
	7.95	0.122	65.16	0.1	58.89	-9.6	-18.3	0.2	52.30	-19.7	35.6	0.2	53.00	-18.7	-33.8	0.2	53.00	-18.7	-33.8
3rd																			
	2.65	0.05	58.9	0.04	66.3	?	?	0.05	53	-10	-19	0.06	48.2	-18.2	-33.1	0.06	48.2	-18.2	-33.1
2nd																			
	4.11	0.04	117	0.05	87.5	?	?	0.05	82.2	-3	-51	0.06	74.7	-36.4	-59.5	0.06	74.7	-36.4	-59.5
Ground																			

Table 4.21 Same as Table 4.12 but for Northridge Aftershock, March 1994

		EW Motions	
		t < 26 s	
(1)	(2)	(3a)	(3b)
Floor	h_i - m	τ_i - s (mean)	ν_i - m/s
Roof			
	5.29	0.107	49.44
6th			
	7.95	0.120	66.25
3rd			
	2.65	0.040	66.25
2nd			
	4.11	0.042	99.86
Ground			

Table 4.22 Same as Table 4.12 but for Northridge Aftershock, December 1994

		EW Motions	
		t < 26 s	
(1)	(2)	(3a)	(3b)
Floor	h_i - m	τ_i - s (mean)	ν_i - m/s
Roof			
	5.29	0.095	55.68
6th			
	7.95	0.116	68.53
3rd			
	2.65	0.036	73.61
2nd			
	4.11	0.022	186.82
Ground			

Table 4.23 Equivalent shear wave velocities of a uniform shear beam, v_{eq}, and fundamental fixed-base frequencies of vibration, f_1, estimated from the mean wave travel times τ_{tot} over the building height, for for EW motions and for all 11 events and time windows considered. For the San Fernando, Landers, and Northridge earthquakes, the percentage change in f_1 and the equivalent rigidity are also shown.

				EW Motions				
(1a)	(1b)	(1c)	(1d)	(2a)	(2b)	(2c)	(2d)	(2e)
Earthquake	Date	Segment	Time interval	τ_{tot} s	v_{eq} m/s	f_1 Hz	$\Delta f_1 / \Delta f_{1,ref}$ %	$\Delta \mu_1 / \Delta \mu_{1,ref}$ %
San Fernando	02/09/1971	S1	t < 5 s	0.185	108.2	1.35		
		S2	5 < t < 11 s	0.2025	98.9	1.23	-9	-16
		S3	11 < t < 25 s	0.255	78.8	0.98	-27	-47
		S4	25 < t < 40 s	0.305	65.7	0.82	-39	-63
Whitter- aft.	10/04/1987	WA	t < 24 s	0.2075	96.5	1.20		
Pasadena	10/03/1988	PA	t < 24.5 s	0.205	97.7	1.22		
Malibu	01/19//1989	MA	t < 25 s	0.209	95.8	1.20		
Montebello	06/12/1989	MB	t < 24 s	0.1925	104.0	1.30		
Sierra Madre	06/28/1991	SM	t < 23 s	0.2175	92.0	1.15		
Landers	06/28/1992	L1	t < 20	0.1975	101.4	1.27		
		L2	20 < t < 80 s	0.205	97.7	1.22	-4	-7
Big Bear	06/28/1992	BB	t < 40 s	0.215	93.1	1.16		
Northridge	01/17/1994	N1	t < 3 s	0.295	67.9	0.85		
		N2	3 < t < 7 s	0.325	61.6	0.77	-9	-18
		N3	7 < t < 12 s	0.365	54.8	0.68	-19	-35
		N4	12 < t < 25 s	0.38	52.7	0.66	-22	-40
		N5	25 < t < 60 s	0.38	52.7	0.66	-22	-40
Northridge aft.	03/20/1994	A1	t < 26 s	0.31	64.6	0.81		
Northridge aft.	10/06/1994	A2	t < 26 s	0.27	74.1	0.93		

Table 4.24 Values of f_1, estimated from the mean wave travel times, and selected recorded motion parameters for the 19 segments analyzed.

	EW Motions								
(1)	(2)	(3a)	(3b)	(3c)	(3d)	(3e)	(3f)	(3g)	(3h)
Segment	f_1 Hz	a_{max}^{Gnd} cm/s^2	a_{max}^{Roof} cm/s^2	v_{max}^{Gnd} cm/s	d_{max} cm	$\bar{a}_{max}$ * cm/s^2	$d_{max}\omega_1^2$ cm/ s^2	f_1^2 Hz^2	$v_{max}^{Gnd}/(4f_1)$ cm
S1	1.35	119.74	186.78	9.12	1.84	153.26	132.16	1.82	1.69
S2	1.23	129.97	315.30	13.02	4.49	222.64	267.71	1.51	2.65
S3	0.98	118.39	289.14	22.38	7.75	203.76	293.52	0.96	5.71
S4	0.82	23.57	59.87	6.68	2.12	41.72	56.17	0.67	2.04
WA	1.20	52.43	53.59	2.18	0.89	53.01	50.81	1.44	0.45
PA	1.22	32.72	29.92	0.94	0.40	31.32	23.53	1.49	0.19
MA	1.20	19.83	28.20	0.93	0.32	24.01	18.00	1.44	0.19
MB	1.30	21.33	27.36	0.80	0.18	24.35	11.95	1.69	0.15
SM	1.15	62.05	57.90	2.76	1.41	59.97	73.58	1.32	0.60
L1	1.27	28.22	125.02	5.25	2.93	76.62	186.16	1.61	1.03
L2	1.22	39.97	116.79	10.26	3.18	78.38	186.91	1.49	2.10
BB	1.16	23.48	54.18	3.02	1.60	38.83	84.64	1.35	0.65
N1	0.85	97.77	104.33	5.80	2.00	101.05	57.11	0.72	1.71
N2	0.77	389.34	435.78	39.61	16.34	412.56	381.97	0.59	12.86
N3	0.68	442.22	563.20	51.06	22.64	502.71	412.88	0.46	18.77
N4	0.66	187.86	232.62	25.90	13.61	210.24	233.73	0.44	9.81
N5	0.66	42.78	233.21	9.30	14.51	137.99	249.35	0.44	3.52
A1	0.81	137.18	89.98	4.86	1.10	113.58	28.43	0.66	1.50
A2	0.93	60.36	37.53	2.26	0.68	48.95	23.30	0.86	0.61

* $\bar{a}_{max} = \left(a_{max}^{Gnd} + a_{max}^{Roof}\right)/2$

4.3 Analysis of Changes of f_1 and Comparison with f_{sys} During Earthquakes and Ambient Vibration Tests

The results for the equivalent uniform shear wave velocity, v_{eq}, listed in Table 4.23, show that it varied between 108 m/s during the first time interval of the San Fernando earthquake ($t < 5$ s) and 53 m/s during the Northridge earthquake ($12 < t < 60$ s), which corresponds to values of the fundamental fixed-base frequency f_1 of 1.35 Hz and 0.66 Hz. As the values of v_{eq} and f_1 are directly related ($f_1 = v_{eq}/(4H)$), we analyze only f_1.

Figure 4.12 shows a plot of f_1 versus time during the 11 earthquakes. It also shows, the soil-structure system frequency f_{sys} during the same earthquakes, and also during five ambient vibration tests conducted as follows: one tests in 1967 – a year after construction, two tests in 1971 following the San Fernando earthquake – one before and the other one after the repairs (Mulhern and Maley 1973), and two more tests after the Northridge earthquake in 1994 – one before and another one after the March 27 aftershock (Ivanović et al 1999; 2000). The curves for f_1 are hand interpolations/extrapolations of the interval values (shown by open circles) assigned to the central time of the intervals. The curves for f_{sys} are smooth values obtained from the Gabor analysis, after eliminating some variations believed to be due to artifacts (Todorovska and Trifunac 2006a). On the top, the relative roof displacements are plotted on same scale for all events.

It can be seen from Fig. 4.12 that the drop of both f_1 and f_{sys} is the largest during the largest earthquake shaking. It can also be seen that for all earthquakes $f_{sys} < f_1$, consistent with eqn (3.7), and our interpretation of f_1 as estimated in this analysis. However, *their ratio is not uniform*, as suggested by eqn (3.7), which corresponds to a *linear* soil-structure interaction model. Between 1987 (Whittier aftershock) and 1992 (Big Bear earthquake), while f_1 is approximately constant for all events, fluctuating around 1.2 Hz, f_{sys} changed significantly from one earthquake to another, and relative to f_1. Its large fluctuations, between about 0.7 Hz (second segment of Landers earthquake) and 1.1 Hz (Malibu earthquake), are obviously not related to damage. Therefore, f_{sys} should not be used for structural health monitoring and damage detection.

It can be seen from Fig. 4.12 that the estimates of f_{sys} from ambient data in 1967 and in 1971 are all higher than f_{sys} during the earthquake shaking for all 11 events, as expected. These values are also higher than the highest value of f_1, which is in contradiction with eqn (3.7)

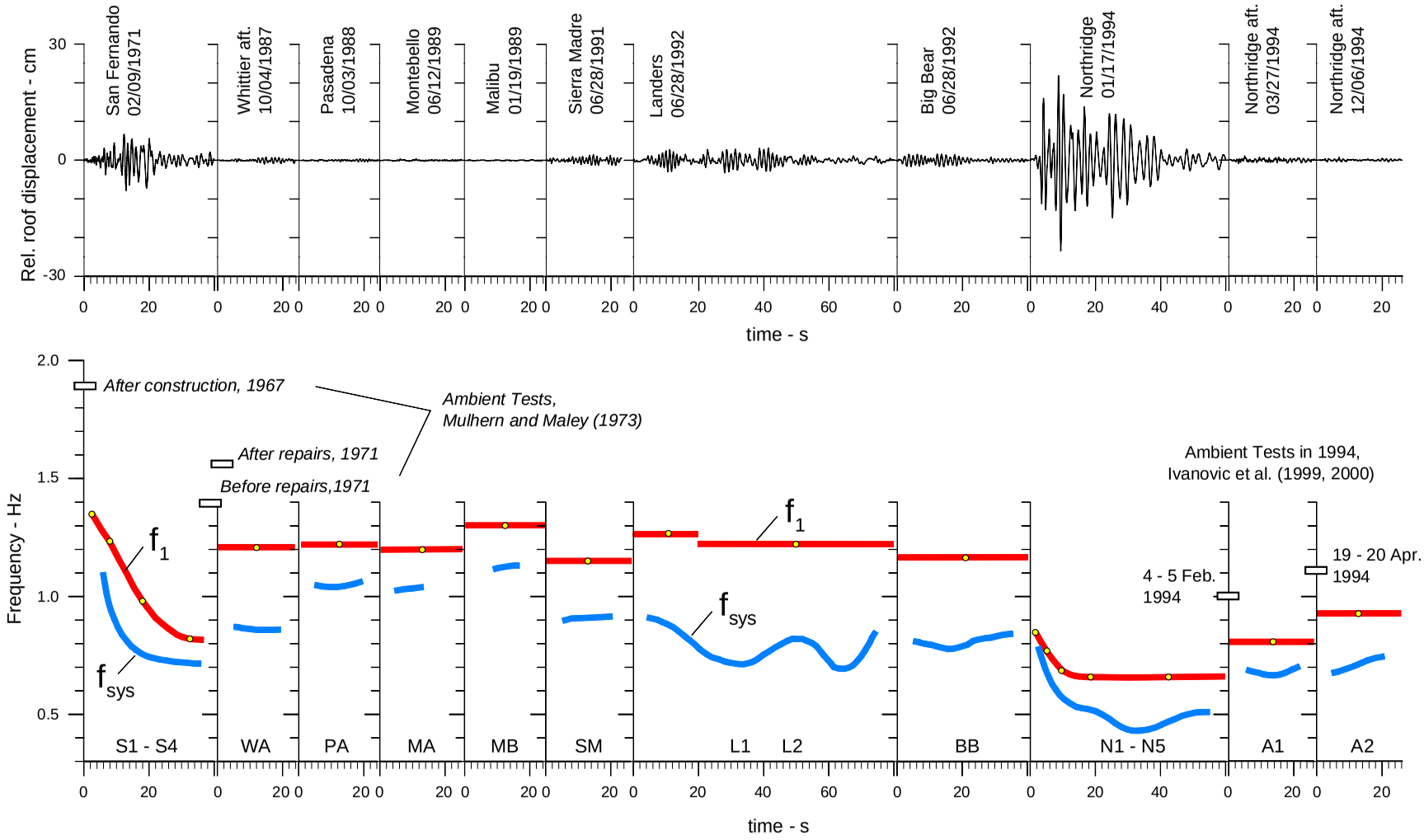

Fig. 4.12 Variations of f_1 and f_{sys} in the Van Nuys building during the 11 earthquakes, between February of 1971 and December of 1994. Measured values of f_{sys} during five ambient vibration tests: (i) in 1967, following construction, (ii) in 1971, after San Fernando earthquake and before repairs, (iii) in 1971 after the repairs (Mulhern and Maley, 1973), (iv) in January of 1994, eighteen days after the Northridge earthquake, and (v) in April of 1994, after the building was restrained by wooden braces (Ivanović et al. 1999, 2000).

describing a linear soil-structure interaction model. The very high estimates of f_{sys} in 1967, which was one year after construction and before any exposure to strong earthquake shaking, could be explained by the fact that the concrete in the structural members was not cracked – hence the columns and beams worked with almost their gross moments of inertia. This all changed permanently during and following the San Fernando earthquake. This value of f_{sys} is larger by 0.5 Hz (26%) than f_1 during the initial time interval ($t < 5$ s) of the San Fernando earthquake.

The value of f_{sys} during the ambient test conducted after the San Fernando earthquake and before repair is larger by 0.57 Hz (41%) than f_1 during the last time interval of the San Fernando earthquake ($25 < t < 40$ s). After the repair, f_{sys} under ambient load increased by 0.17 Hz (by 12%). We also compared the value of f_{sys} from the ambient test conducted after the repair with f_1 during the Whittier aftershock. The latter is smaller by 0.36 Hz, which is 23% of the value of the former.

The relationship is similar for the Northridge earthquake. For both ambient vibration tests, f_{sys} is higher than f_1 during both the Northridge main event and during the two aftershocks. The value of f_{sys} during the ambient tests conducted after the main event and before braces were added is larger by 0.34 Hz than f_1 during the last time interval of the main event ($25 < t < 60$ s), which is 34% of its value. It is also larger by 0.19 Hz (19%) than f_1 during the March aftershock (we do not know if the building had braces during the March aftershock). After the March aftershock and the addition of braces, f_{sys} under ambient loads increased by 0.1 Hz (10%). This value of f_{sys} is larger by 0.17 Hz (16%) than f_1 during the December aftershock. In all of these comparisons of f_{sys} under ambient loads and f_1 during an earthquake, f_{sys} was used as a reference in computing the percentage difference.

This apparent contradiction of higher f_{sys} during ambient tests than f_1 during earthquake shaking could be due to the added stiffness from the nonstructural elements, which participated in the resistance to the ambient loads, but not to the earthquake loads.

4.4 Analysis of Changes of Average Floor Velocities and Stiffnesses

The average floor velocities between sensors, v_i, represent local properties of the building. Fig. 4.13 shows graphically the variations of v_i (listed in Tables 4.12 through 4.22) versus time, over a period of 24 years, between February 1971 and December 1994. For the San Fernando earthquake (recorded by three self contained AR-240 accelerographs; Fig.2.6a), the average wave velocities can be shown only for two segments along the building height – Ground to 4th floor, and 4th floor to Roof. For all other earthquakes, the EW response was recorded at five levels (by five channels of the CR-1 structural array; Fig. 2.6b), and the average wave velocities can be shown for four segments – Ground to 2nd floor, 2nd to 3rd floors, 3rd to 6th floors, and 6th floor to Roof.

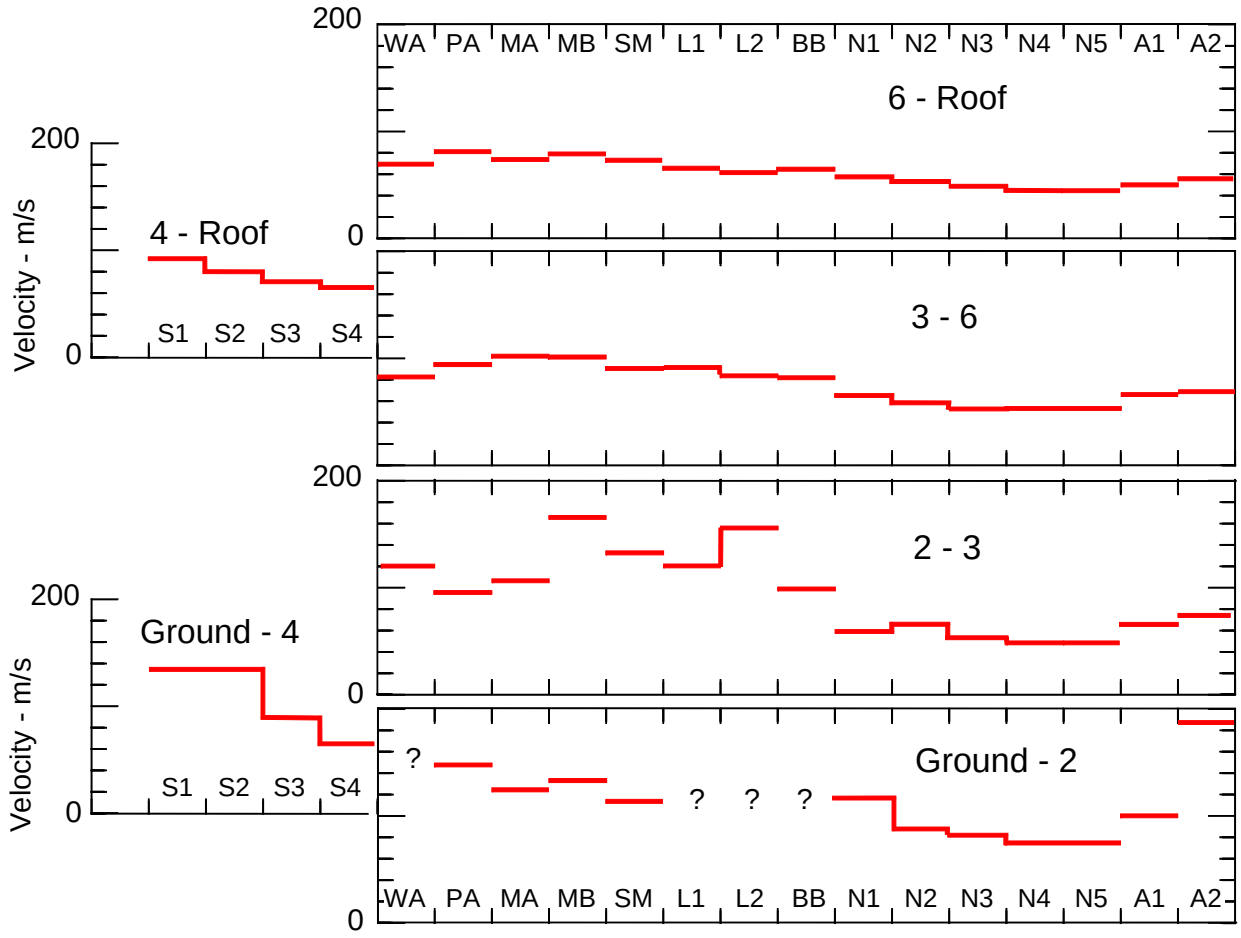

Fig. 4.13. Average shear wave velocities between floors in the Van Nuys building during the 11 earthquakes. The different events and time intervals of the two largest events are identified by a code (see Table 4.23 for identification of the events and time segments).

It can be seen from Fig. 4.13 that, during the strong motion segment of San Fernando earthquake ($t < 30$ to 40 s), v_i between the ground and 4th floor dropped from near 140 m/s to about 70 m/s (–50%). Above the 4th floor, the relative drop of v_i was smaller, from about 90 m/s to 70 m/s (–22%).

The shaking amplitudes during the period from 1987 to 1992 were small and, except perhaps for the LA event, the building responded in an essentially linear manner. As Fig. 4.13 shows, during this time the velocities in the building fluctuate, which we interpret to be mainly due to errors in the manual reading of the arrival times, for impulses propagating up and down the building (Figs 4.1 through 4.11 and Tables 4.1 through 4.11), and due to undocumented changes in the building environment (e.g. Todorovska and Al-Rjoub 2006). These fluctuations are larger for the lower floors, for which the relative error in the estimation of the travel times was larger (due to the smaller distance between sensors). For that reason, the velocities between the ground and 4th floor are not shown for the WA, L1, L2, and BB events, as unreliable. The accuracy of the estimated propagation times can be improved by modeling in terms of ray tracing in the building, but this is beyond the scope of this analysis.

The average wave velocities experienced another significant drop during the Northridge earthquake in 1994. Between the ground and 2nd floor, for example, the velocity dropped from about 120 m/s to near 70 m/s (–40%). We believe this drop is a result of the damage in the building (Figs. 2.3 and 2.4). Figure 4.13 shows an increase in the wave velocities throughout the building during the Northridge aftershocks, which we believe is a consequence of the increase in stiffness due to the wooden braces. These braces were added following the earthquake, to strengthen the building until completion of the repairs in 1996 (see Figs. 2.4 and 2.5; Trifunac and Hao 2001).

Figure 4.14 shows the changes of the average floor velocities, v_i, and of the average floor rigidities, μ_i, versus time during the 1971 San Fernando and Northridge earthquakes (see Tables 4.12 and 4.20). Both quantities have been normalized with respect to their values in the corresponding initial time segment. It can be seen that, during the San Fernando earthquake, the large drop in stiffness occurred gradually – during the first 30 s, while, during the Northridge earthquake, this drop was rapid – taking place during the first 10 s of strong motion. During the San Fernando earthquake, the average stiffness between the ground and 4th floor dropped by about 80%, while during the Northridge it dropped by about 60%. The reductions in stiffness at higher elevations in the building were smaller, about 50% for the San Fernando and about 30% to 40% for the Northridge earthquake.

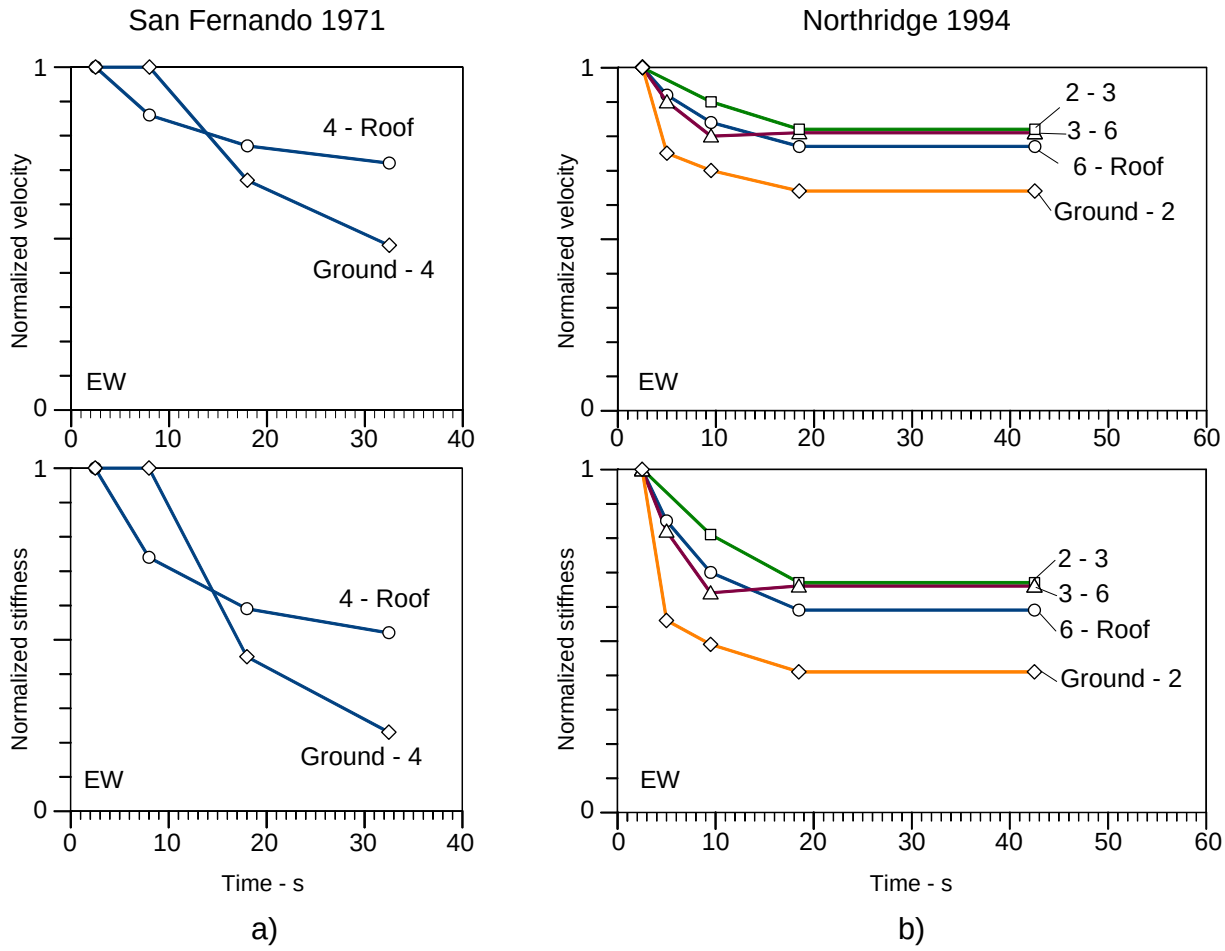

Fig. 4.14 Reduction of the average wave velocities (top) and stiffness (bottom) between floors during the (a) 1971 San Fernando and (b) 1994 Northridge earthquakes.

The observed damage in the building following the Northridge earthquake was more severe than during the San Fernando earthquake, contrary to the relative drop in stiffness implied by the analysis of travel times. We interpret this to be due to the fact that the building was already weakened at the time of the Northridge earthquake, by repeated shaking from the previous earthquakes. Although the building was repaired after the San Fernando earthquake, numerous small cracks remained, which were reactivated and enlarged by the subsequent earthquakes between 1987 and 1992. Thus, the severe damage occurred during the Northridge earthquake with smaller relative reduction of stiffness.

4.5 Global and Local Indicators of Damage - When Does Damage Occur?

The trends of f_1 shown in Fig. 4.12 suggest that changes of interval values of f_1 during strong shaking can be used as a simple *global* indicator of damage. A drop of f_1 by more than certain percentage (say about 20% for the Van Nuys building), relative to the value of the initial time interval of weaker shaking, would be an indicator that damage has occurred. Such an algorithm, implemented in a real time health monitoring system, would have indicated that damage occurred in the Van Nuys building during the San Fernando and the Northridge earthquakes as early as about 10 s after trigger of strong motion recorders. We note here that such a rule applied to f_{sys} would not work, since it would have resulted in a false alarm during the Landers earthquake. Although eqn. (3.7) suggests a constant relationship between f_{sys} and f_1 during linear and almost linear levels of response, that is not necessarily true for strong earthquake shaking, as indicated by this analysis.

The changes of the interval values of the average floor velocities between sensors, v_i, can be used also as *local* indicators of damage. For the Van Nuys building, the observed drops in v_i: (a) during the San Fernando earthquake of about 30% (from time interval S2 to S3) between the Ground and 4$^{\text{th}}$ floor, and (b) during the Northridge earthquake of more than 20% (from time interval N1 to N2) between Ground and 2$^{\text{nd}}$ floor, and 3$^{\text{rd}}$ and 6$^{\text{th}}$ floors, are all consistent with the locations of the observed damage. The large fluctuations of v_i between the 2$^{\text{nd}}$ and 3$^{\text{rd}}$ floors for the WA, PA, MA, MO, SM L1, L2, and BB events, appear to have been caused by the uncertainty in reading the impulse arrival times. Such large fluctuations can be eliminated or reduced significantly by fitting a model for the propagation times, which is beyond the scope of this work. Obviously, denser seismic monitoring arrays in buildings with a smart configuration of sensors, and algorithms based on wave propagation times can be a powerful tool for localized health monitoring and damage detection.

4.6 Force-Displacement Relationships Inferred From Wave Travel Times

The true nature of the earthquake response of virtually all structures can be described best in terms of *nonlinear* wave propagation (Gičev and Trifunac 2006). The engineering formulation of the corresponding *linear* problem has instead tended to use the vibrational approach, formulated as the Response Spectrum Superposition method proposed in the early 1930s (Biot 1932; 1933; 1934; 1941; 1942; Trifunac 2003; 2006). A general theory for nonlinear response of multi degree-of-freedom systems has yet to be developed. In the meantime, simplified representations and approximate gross modeling of structures, formulated around various extensions of the response spectrum method, are used in seismic design. One such simplified

method for estimation of nonlinear response is push over analyses. A typical push over analysis presents the base shear coefficient versus the displacement of the top of the structure, and describes a "force-displacement relationship" of an "equivalent" single degree of freedom system. The results of our analysis can also be viewed in such a form, for comparison with previous results, and for understanding of how the two approaches compare. For that purpose, we show in Figures 4.15, 4.16 and 4.17 plots involving various parameters of the response to the 11 earthquakes and the fixed-base frequency, f_1, estimated from the wave travel time (see Table 4.24).

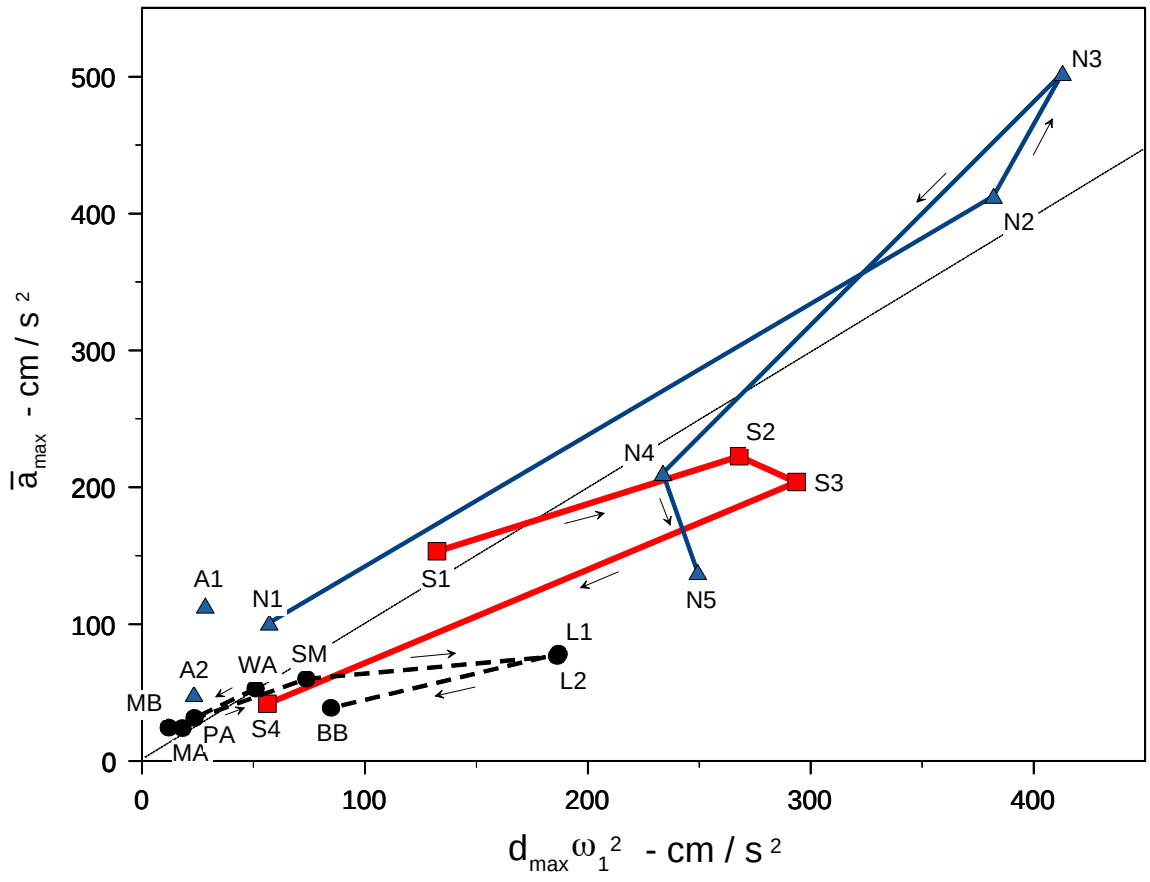

Fig. 4.15 Average peak inertial force versus peak equivalent spring force (both per unit mass) during the 11 earthquakes. For the 1971 San Fernando and 1994 Northridge earthquakes, these values were computed respectively for four and five time segments (see Table 4.23 for identification of the time intervals).

Let $\bar{a}_{max}$ be the average value of the peak interval acceleration, $\bar{a}_{max} = (a_{max}^{Gnd} + a_{max}^{Roof})/2$ and let m be the mass of the building. Then $m\bar{a}_{max}$ is a measure of the peak inertial force acting on the structure. The peak inertial force is approximately equal to the peak restoring force, which is

proportional to kd_{max}, where d_{max} is the peak *relative* displacement and k is the corresponding stiffness. Recalling that $\omega_n^2 = k/m$, where ω_n is the circular natural frequency of an oscillator, we can expect that $\bar{a}_{max} \approx d_{max}\omega_1^2$ in both the linear and the nonlinear range of response for all time intervals considered in this analysis. Fig. 4.15 shows $\bar{a}_{max}$ versus $d_{max}\omega_1^2$, where $\omega_1 = 2\pi f_1$ was computed using f_1 from the travel time analyses. It can be seen that all data points in this figure lie approximately along a 45° line, which confirms that f_1 estimated from wave travel times is physically meaningful. The departures from a straight line are at most about a factor of

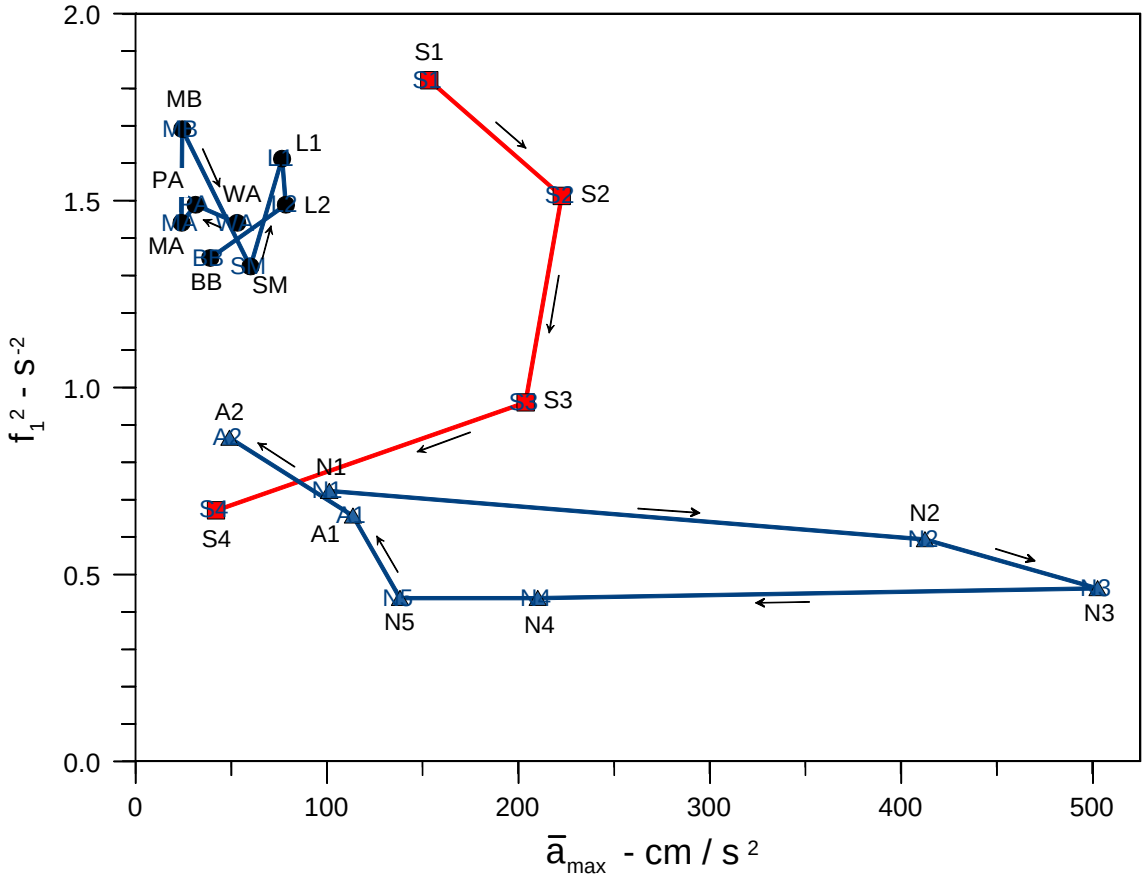

Fig. 4.16 Normalized secant modulus versus average inertial force during the eleven earthquakes (see Table 4.23 for identification of the time intervals).

two, and include the influence of the soil-structure interaction (the effects of which on the peak relative response d_{max} could not be separated, due to inadequate instrumentation), the measurement errors in the estimates of f_1, and the occurrence of the peak ground and roof accelerations, and the peak roof displacements at different times.

Fig. 4.16 shows f_1^2 versus $\bar{a}_{max}$, where the former is a measure of the secant modulus of the equivalent stiffness of the building ($\approx m\bar{a}_{max}/d_{max} \approx m\omega_n^2 d_{max}/d_{max} = m4\pi^2 f_1^2 \sim f_1^2$), and the latter is a measure of the force producing the deformation ($\approx m\bar{a}_{max} \sim \bar{a}_{max}$). It can be seen that the data points corresponding to the nonlinear (damaging) responses during San Fernando and Northridge earthquakes are clearly separated from those corresponding to the essentially linear response during the WA, PA, MA, MO, SM, L1, L2, and BB events/intervals. The relatively

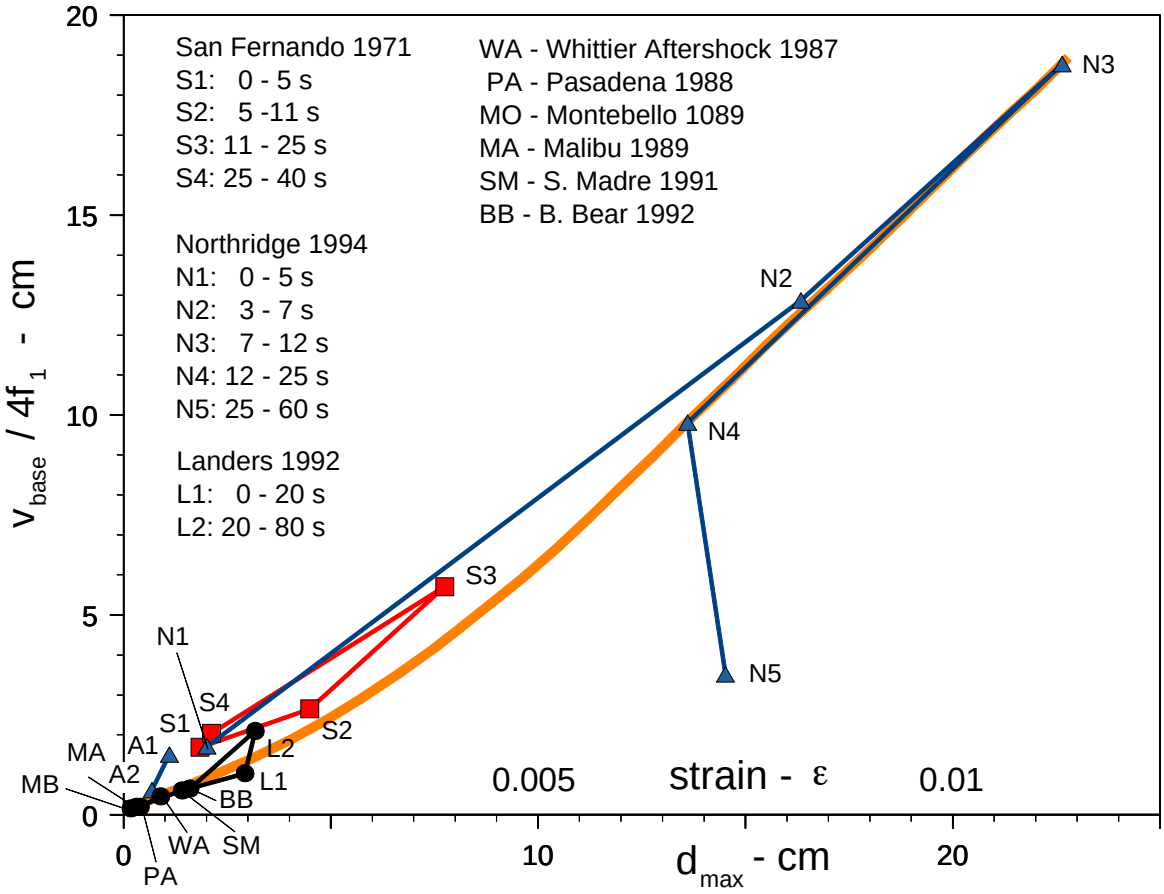

Fig. 4.17 Peak linear shear strain versus peak average drift in the Van Nuys building during the 11 earthquakes.

small amplitude of f_1^2 for N1 (the first time interval of the Northridge earthquake) is probably due to the rapid growth of the strong motion amplitudes in this interval, but could also mean that the building was already "softer" before the Northridge earthquake, because of the accumulated effects of all preceding earthquakes. Both clockwise loops S1-S2-S3-S4, and N1-N2-N3-N4-N5 are affected by the soil-structure interaction to a degree that cannot be quantified by this analysis.

Finally, Fig. 4.17 shows $v_{\text{base}} / 4 f_1$ versus $d_{\max}$, where the former is a measure of the average linear strain associated with a one-dimensional shear wave transmitted into the building ($\sim v_{\text{base}} / \overline{\beta} = v_{\text{base}} /(4Hf_1)$, where v_{base} is the peak interval velocity at the ground floor, and $\overline{\beta} = 4Hf_1$ is the average shear wave velocity in the building), and the latter is a measure of the peak average drift in the building ($\approx d_{\max} / H$, where H is the building height). Therefore we expect $v_{\text{base}} / 4 f_1 \sim d_{\max}$. Indeed, all the data points lie approximately along a straight line. For the Van Nuys building, $H = 20$ m and consequently $d_{\max}$ = 20 cm corresponds to average strain of 1%. From the coordinates of the points in Fig. 4.17 that correspond to the damaging events/time intervals, it can be seen that *the damage began to occur for strains exceeding 0.002 to 0.003, as would be expected for a reinforced concrete structure*. The largest average strains for this group of eleven earthquakes occurred during the N3 segment of the Northridge earthquake.

5. DUSCUSSION AND CONCLUSIONS

This report describes our second exploratory study of a new structural health monitoring method, based on detecting changes in the stiffness of the structural members, by measuring changes in the travel times of seismic waves propagating through these members. The wave travel times are estimated from impulse response analysis. These changes can also be translated into changes of the fundamental fixed-base frequency of the structure. In both studies, we applied the method to strong motion data recorded in buildings that have been damaged. The subject of our first study was the transverse and longitudinal response of the Imperial County Services building, in El Centro, California, which was a 6-story reinforced concrete building damaged by the Imperial Valley earthquake of 1979 (Todorovska and Trifunac 2006c). The subject of our current study is the longitudinal (EW) response of a 7-story reinforced concrete hotel building located in the city of Van Nuys of the Los Angeles metropolitan area, which was damaged by the San Fernando earthquake of in 1971, and by the Northridge earthquake of 1994. For the latter building, we also analyzed the response for 9 other earthquakes. For both buildings, results for the system frequencies measured during ambient vibration tests are also available.

For the damaging earthquakes, for both buildings we computed impulse responses by deconvolution of the recorded earthquake response, and measured the wave travel times within consecutive time windows. For the Van Nuys building, we did the same also for the 1992 Landers earthquake, during which the strong motion data shows a reduction of the system frequency, but no damage was observed. For all of these events, we expressed the changes in the wave velocities and rigidities relative to the initial time window, which we used as baseline data. Thus, the method did not require response data measured before the earthquake. This method enabled us to detect both *global* changes, by monitoring the changes of the fixed-base frequency within the different time windows, and *local* changes in rigidity, by monitoring the changes in wave travel time between sensors. For the Van Nuys building, the data from the other earthquakes that did not cause visible damage provided useful information about the amplitude dependence of the monitored local and global quantities.

In both of our exploratory studies, we applied the impulse response method in its most rudimentary form, based on several simplifying assumptions. The first assumption is that one-dimensional wave propagation up and down the structure can capture the principal features of the response, and that side reflections of the non-vertically propagating waves (Todorovska et al. 1988) can be neglected. Second assumption is that it is sufficient to work only with the recorded horizontal translations. Another group of assumptions is related to the transmittal of the incident waves through the foundation. In that regard, we assumed that the effects associated with the horizontal propagation of seismic waves incident through the foundation can be neglected (Gičev and Trifunac, 2006; Trifunac et al. 1999a), that the structural response resulting from warping

and deformation of the foundation can be neglected (Gičev, 2005), and that the rotational waves in the building, caused by soil-structure-interaction, and by the rotational components of the ground motion (associated with body P, and SV waves, and Rayleigh surface waves) can be neglected. Finally, we did not consider explicitly the detailed nature of the contributions of torsion and of rocking to the recorded horizontal EW translations.

The spatial resolution of the method depends on the number and the separation distance of the sensors, while its temporal resolution depends on the length of the time window chosen for the analysis. The wave travel times we measured by reading manually the impulse arrival times at different stations, with error of about $\Delta\tau \approx 0.01$ s. As it can be seen from Table 4.23, the wave travel time over the height of the building changed during the San Fernando earthquake between $\tau_{tot} = 0.185$ s and 0.305 s (or by $\Delta\tau_{tot} = 0.12$ s), and during the Northridge earthquake it changed between $\tau_{tot} = 0.295$ s and 0.38 s (or by $\Delta\tau_{tot} = 0.085$ s). During the other smaller events, $\tau_{tot} \sim 0.2$ s. This implies that the error in reading the pulse arrival times, $\Delta\tau$, is about 20-30 times smaller than τ_{tot}, and about 10 time smaller than the change in travel time $\Delta\tau_{tot}$ interpreted to be due to damage. The determination of the wave travel times can be automated by fitting a model to the data.

The results in this work confirm the findings of our first study (Todorovska and Trifunac 2006c) that, despite the simplifying assumptions, even for time windows as short as about 5 s, the method yields physically meaningful impulse responses and wave travel times. The estimates of fixed-base frequency from the measured wave travel times we found to be consistent with the concurrent estimates of soil-structure system frequency. Finally, the changes in *fixed-base* frequency, f_1, and average floor velocities between sensors, v_i we found to be consistent with the observed earthquake damage. In contrast, we found that tracking changes in the soil-structure system frequency can produce misleading inferences about the occurrence of damage, and can lead to false alarms. Specifically, we found that, during the San Fernando earthquake, f_1 decreased by about 40% (relative to is value within the first 5 s from trigger), which corresponds to a decrease in the global rigidity of about 63% (see Table 4.23). During the Northridge earthquake, f_1 decreased by about 22% (relative to is value within the first 3 s from trigger), which corresponds to a decrease in the global rigidity of about 40%. We also found that, although the first system frequency, f_{sys} was always smaller than f_1, their difference varied (see Fig. 4.12), contrary to what one could expect from a linear soil-structure interaction model (eqn. (3.7)). The local changes of rigidity, as implied by this method, are as follows. During the San Fernando earthquake, the rigidity decreased by about 77% between the Ground and 4th floors, and by about 48% between the 4th floor and roof (see Table 4.12). During the Northridge earthquake, the rigidity decreased by about 60% between Ground and 2nd floors, by about 33%

between 2nd and 3rd floors, and between 3rd and 6th floors, and by about 41% between the 6th floor and Roof (see Table 4.20).

We conclude that the analysis of wave travel times in a building undergoing damaging response via impulse response functions, computed from the recorded seismic response, can provide useful and reliable information about the degree and spatial distribution of the changes in its stiffness. Clearly, this method will be a useful tool for structural health monitoring, and should be further improved and refined.

REFERENCES

1. Biot, M.A. (1932). Vibrations of Buildings During Earthquake, Chapter II in *Ph.D. Thesis No. 259*, entitled "Transient Oscillations in Elastic System," Aeronautics Department, Calif. Inst. of Tech., Pasadena, California.

2. Biot, M.S. (1933). Theory of Elastic Systems Vibrating Under Transient Impulse With an Application to Earthquake-Proof Buildings, *Proc. National Academy of Sciences*, **19**(2), 262–268.

3. Biot, M.A. (1934). Theory of Vibration of Buildings During Earthquakes, *Zeitschrift für. Angewandte Matematik und Mechanik*, 14(4), 213–223.

4. Biot, M.A. (1941). A Mechanical Analyzer for the Prediction of Earthquake Stresses, *Bull. Seism. Soc. Amer*., **31**, 151–171.

5. Biot, M.A. (1942). Analytical and Experimental Methods in Engineering Seismology, *ASCE Transactions*, **108**, 365–408.

6. Blume, J.A., and Assoc. (1973). Holiday Inn, Chapter 29 in "San Fernando, California Earthquake of February 9, 1971", Volume I, Part A, U.S. Dept. of Commerce, National Oceanic and Atmospheric Administration, Washington, D.C.

7. Browning, J.A., Li, R.Y., Lynn, A., and Moehle, J.P. (2000). Performance assessment for a reinforced concrete frame building, *Earthquake Spectra*, **16**(3), 541-555.

8. Chang P.C., Flatau A., Liu S.C. (2003). Review paper: health monitoring of civil infrastructure, *Structural Health Monitoring*, **2**(3), 257-267.

9. De la Llera, J.C., Chopra, A.K., and Almazan, J.L. (2001). Three-dimensional inelastic response of an RC building during the Northridge earthquake. *J. Structural Eng.*, ASCE, **127**(5), 482-489.

10. Doebling S.W., Farrar C.R., Prime M.B., Shevitz D.W. (1996). Damage identification and health monitoring of structural and mechanical systems from changes in their vibration characteristics: a literature review, *Report LA-13070-MS*, Los Alamos National Laboratory, Los Alamos, NM.

11. Gičev, V. (2005). Investigation of soil-flexible foundation-structure interaction for incident plane SH waves, *Ph.D. Dissertation*, Dept. of Civil Engineering, Univ. Southern California, Los Angeles, California.

12. Gicev, V., and Trifunac, M.D. (2006). Permanent Deformations and Strains in a Shear Building Excited by a Strong Motion Pulse, *Soil Dynamics and Earthquake Engineering,* (in press) (2006).

13. Graizer, V. (1997). Personal Communication.

14. Haddadi, H.R., and Kawakami, H. (1998). Modeling wave propagation by using normalized input-output minimization (NIOM) method for multiple linear systems, *Structural Eng./ Earthquake Eng.*, JSCE, **15**(1), 29-39

15. Hudson, D.E., Trifunac, M.D., Brady, A.G., and Vijayaraghavan, A. (1971). Strong-motion earthquake accelerograms, II, corrected accelerograms and integrated velocity and displacement curves, *Report EERL 71-51*, Earthquake Eng. Res. Lab., Calif. Inst. of Tech., Pasadena, California.

16. Islam, M.S. (1996). Analysis of the response of an instrumented 7-story nonductile concrete frame building damaged during the Northridge earthquake, *Professional paper 96-9*, Los Angeles Tall Building Structural Design Council, 1996 Annual Meeting.

17. Ivanović, S., Trifunac, M.D., Novikova, E.I., Gladkov, A.A., and Todorovska, M.I. (1999). Instrumented 7-storey reinforced concrete building in Van Nuys, California: Ambient vibration survey following the damage from the 1994 Northridge Earthquake, *Dept. of Civil Eng., Rep. No. CE 99-03*, Univ. of Southern California, Los Angeles, California.

18. Ivanović, S., Trifunac, M.D., Novikova, E.I., Gladkov, A.A., and Todorovska, M.I. (2000). Ambient vibration tests of a seven story reinforced concrete building in Van Nuys, California, damaged by the 1994 Northridge Earthquake, *Soil Dynamics and Earthquake Eng*., **19**(6), 391-411.

19. Ivanović, S., Trifunac, M.D., and Todorovska, M.I. (2001). On identification of damage in structures via wave travel times, *Proc. NATO Workshop on Strong Motion Instrumentation for Civil Engineering Structures*, June 2-5, 1999, Istanbul Turkey, Kluwer Academic Pub., Dordrecht, 447-468.

20. Kanai, K. (1965). Some new problems of seismic vibrations of a structure, *Proc. Third World Conf. on earthquake Engineering*, Auckland and Wellington, New Zealand, January 22-February 1, 1965, pp. II-260 to II-275.

21. Lee, V.W, and Trifunac, M.D. (1990). Automatic digitization and processing of accelerograms using PC, *Dept. of Civil Eng. Report 90-03*, Univ. Southern California, Los Angeles, California.

22. Li, Y.R., and Jirsa, J.O. (1998). Nonlinear analyses of an instrumented structure damaged in the 1994 Northridge earthquake, *Earthquake Spectra*, **14**(2), 265-283.

23. Ma, J., and Pines, D.J. (2003). Damage detection in a building structure model under seismic excitation using dereverberated wave machines, *Engineering Structures*, **25**, 385-396.

24. Mulhern, M.R., and Maley, R.P. (1973). Building period measurements before, during and after the San Fernando, California, earthquake of February 9, 1971, U.S. Depart. Of Commerce, National Oceanic and Atmospheric Administration, Washington D.C., Vol. I, Part B, 725-733.

25. Şafak, E. (1999). Wave propagation formulation of seismic response of multi-story buildings. *J. of Structural Eng*., ASCE, **125**(4), 426-437.

26. Snieder, R., and Şafak, E. (2006). Extracting the building response using interferometry: theory and applications to the Millikan Library in Pasadena, California, *Bull. Seism. Soc. Am*., **96**(2), 586-598.

27. Todorovska, M.I., and Lee, V.W. (1989). Seismic waves in buildings with shear walls or central core, *J. Engrg Mech.*, ASCE, **115**(12), 2669-2686.

28. Todorovska, M.I and Al-Rjoub, Y. (2006). Effects of Rainfall on Soil-Structure System Frequency: Examples based on Poroelasticity and a Comparison with Full-Scale Measurements, *Soil Dynamics and Earthquake Engineering*, **26**(6-7), 708-717.

29. Todorovska, M.I., and Trifunac, M.D. (1989). Antiplane earthquake waves in long structures, *J. Engrg Mech.*, ASCE, **115**(12), 2687-2708.

30. Todorovska, M.I., and Trifunac, M.D. (1990). A note on the propagation of earthquake waves in buildings with soft first floor, *J. Engrg Mech*., ASCE, **116**(4), 892-900.

31. Todorovska, M.I., and Trifunac, M.D. (1997a). "Amplitudes, polarity and time of peaks of strong ground motion during the 1994 Northridge, California, earthquake", *Soil Dynam. and Earthquake Engrg*, **16**(4), 235-258.

32. Todorovska, M.I., and Trifunac, M.D. (1997b). "Distribution of pseudo spectral velocity during the Northridge, California, earthquake of 17 January, 1994", *Soil Dynam. and Earthquake Engrg*, **16**(3), 173-192.

33. Todorovska, MI, and Trifunac, M.D. (2006a). Earthquake damage detection in the Imperial County Services Building I: the data and time-frequency analysis, submitted for publication.

34. Todorovska, MI, and Trifunac, M.D. (2006b). Earthquake damage detection in the Imperial County Services Building II: analysis of novelties via wavelets, *Soil Dynam. and Earthquake Engrg* (submitted for publication).

35. Todorovska, M.I. and Trifunac, M.D. (2006c). Earthquake damage detection in the Imperial County Services Building III: analysis of wave travel times via impulse response functions, *Soil Dynam. and Earthquake Engrg* (submitted for publication).

36. Todorovska, M.I., Lee, V.W., and Trifunac, M.D. (1988). Investigation of earthquake response of long buildings, *Dept. of Civil Engineering Report CE 88-02*, Univ. of Southern California, Los Angeles, California.

37. Trifunac, M.D. (1974). A three-dimensional dislocation model for the San Fernando, California, Earthquake of February 9, 1971, *Bull. Seism. Soc. Amer*, **64,** 149-172.

38. Trifunac, M.D. (2003). 70-th Anniversary of Biot Spectrum, 23-rd Annual ISET Lecture, *J. Indian Society of Earthquake Technology*, **40**(1), 19-50.

39. Trifunac, M.D. (2006). Biot Response Spectrum, *Soil Dynamics and Earthquake Engineering,* **26**(6-7), 491-500.

40. Trifunac, M.D., and Hao, T.Y. (2001). 7-story reinforced concrete building in Van Nuys, California: photographs of the damage from the 1994 Northridge earthquake, *Dept. of Civil Eng. Report CE 01-05*, Univ. of Southern California, Los Angeles, California.

41. Trifunac, M.D., and Ivanović, S.S. (2003). Analysis of drifts in a seven-story reinforced concrete structure, *Dept. of Civil Eng. Report CE 03-01*, Univ. of Southern California, Los Angeles, California.

42. Trifunac, M.D., and Lee, V.W. (1973). Routine computer processing of strong motion accelerograms, *Earthquake Eng. Res. Lab., Report EERL 73-03*, Calif. Inst. of Tech., Pasadena, California.

43. Trifunac, M.D. and Lee, V.W. (1979). Automatic digitization and processing of strong-motion accelerograms, Part I-pp. 1-259, Part II pp. 260-379, *Dept. of Civil Eng. Report CE 79-15*, Univ. of Southern California, Los Angeles, California.

44. Trifunac, M.D., and Todorovska, M.I. (1997a). Northridge, California, earthquake of 1994: density of red-tagged buildings versus peak horizontal velocity and intensity of shaking, *Soil Dynam. and Earthquake Engrg*, **16** (3), 209-222.

45. Trifunac, M.D., and Todorovska, M.I. (1997b). Northridge, California, earthquake of 1994: density of pipe breaks and surface strains, *Soil Dynam. and Earthquake Engrg,* **16** (3), 193-207.

46. Trifunac, M.D., and Todorovska, M.I. (1998). Damage distribution during the 1994 Northridge, California, earthquake in relation to generalized categories of surficial geology, *Soil Dynam. and Earthquake Engrg,* **17**(4), 238-252.

47. Trifunac, M.D., and Todorovska, M.I. (1999). Reduction of structural damage by nonlinear soil response, *J. Struc. Engrg*., ASCE, 125(1), 89-97.

48. Trifunac, M.D., and Todorovska, M.I. (2001). Recording and interpreting earthquake response of full-scale structures, *Proc. NATO Workshop on Strong Motion Instrumentation for Civil Engineering Structures*, June 2-5, 1999 Istanbul, Turkey, Kluwer Pub. Dordreeht, 131-155.

49. Trifunac, M.D., Todorovska, M.I., and Ivanović, S.S. (1994). A note on distribution of uncorrected peak ground accelerations during the Northridge, California, earthquake of 17 January, 1994, *Soil Dynam. and Earthquake Engrg*, **13**(3), 187-196.

50. Trifunac, M.D., Todorovska, M.I., and Ivanović, S.S. (1996). Peak velocities and peak surface strains during Northridge, California, Earthquake of 17 January 1994, *Soil Dynamics and Earthquake Engineering,* **15**(5), 301-310.

51. Trifunac, M.D., Brady, A.G. and Hudson, D.E. (1973). Strong motion earthquake accelerograms, digitized and plotted data, Volume II, Part C, *Earthquake Eng. Res. Lab., Report EERL-72-51*, Calif. Institute of Tech., Pasadena, California.

52. Trifunac, M.D., Ivanović, S.S., Todorovska, M.I., Novikova, E.I., and Gladkov, A.A. (1999a). Experimental evidence for flexibility of a building foundation supported by concrete friction piles, *Soil Dynam. and Earthquake Eng*., **18**, 169-187.

53. Trifunac, M.D., Ivanović, S.S., and Todorovska, M.I. (1999b). Seven story reinforced concrete building in Van Nuys, California: strong motion data recorded between 7 Feb. 1971 and 9 Dec., 1994, and description of damage following Northridge 17 January 1994 earthquake, *Dept. of Civil Eng. Rep. CE 99-02*, Univ. of Southern California, Los Angeles, California.

54. Trifunac, M.D., Ivanović, S.S., and Todorovska, M.I. (2001a). Apparent periods of a building, Part I: Fourier analysis, *J. Struct. Engrg,* ASCE, **127**(5), 517-526.

55. Trifunac, M.D., Ivanović, S.S., and Todorovska, M.I. (2001b). Apparent periods of a building, Part II: time-frequency analysis, *J. Struct. Engrg*, ASCE, **127**(5), 527-537.

56. Trifunac, M.D., Ivanović, S.S. and Todorosvka, M.I. (2003). Wave propagation in a seven-story reinforce concrete building: III damage detection via changes in wave numbers, *Soil Dyn. And Earthquake Eng.*, **23**(1), 65-75.

57. Wald, D.J., Heaton, T.H. and Hudnut. K.W. (1996). The slip history of the 1994 Northridge, California, earthquake determined from strong motion, teleseismic, GPS and leveling data, *Bull. Seism. Soc. Amer*., **86**(1B), S49-S70.